waterloopkundig laboratorium
delft hydraulics laboratory

wave driven coastal currents

currents in a closed basin

H.G. Wind

progress report

R 1174-9

December 1982

tow
toegepast onderzoek
waterstaat

CONTENTS

CONTENTS (continued)

LIST OF TABLES

LIST OF FIGURES

BIBLIOGRAPHY

APPENDICES

NOTATION

a	wave amplitude	m
c	wave celerity	m/s
c_f, C	frictional coefficient	-
d	undisturbed water depth	m
E	energy density per unit area	Nm^{-1}
g	acceleration due to gravity	ms^{-2}
h	mean water depth	m
H	wave height	m
k	wave number	m^{-1}
I, K	Bessel functions	-
L	length of region	m
m	beach slope	-
n	shoaling coefficient	-
N	coefficient in eddy viscosity	-
p, q	volume transports per unit width in x and y direction	$m^2 s^{-1}$
P	viscosity-friction ratio	-
r	frictional parameter	ms^{-1}
Re	Reynolds number	-
$R_{\Delta x}$	cell Reynolds number	-
S_{xx} etc	radiation stress	Nm^{-2}
t	time	s
T	wave period	s
u, v	velocity components	ms^{-1}
x, y	horizontal co-ordinates	m
z	vertical co-ordinate	m
z_b	bottom level	-
γ	breaking index	-
Δt	time step	s
Δx, Δy	mesh-widths	m
ε	eddy viscosity	$m^2 s^{-1}$
η	water level variation due to waves	m
Θ	weighing coefficient in difference scheme	-
λ	2π/wave length of perturbation	m^{-1}
ζ	water level relative to undisturbed level	m
ρ	fluid density	kgm^{-3}

NOTATION (continued)

τ_{bx}, τ_{by}	components of bottom shear stress	Nm^{-2}
τ_{sx}, τ_{sy}	components of surface shear stress	Nm^{-2}
τ_{xx} etc	components of stresses in vertical planes	Nm^{-2}
ϕ	direction of wave propagation	-
ω	vorticity	-

WAVE DRIVEN COASTAL CURRENTS; CURRENTS IN A CLOSED BASIN

1. Introduction

In the period 1978 - 1980 a numerical model, named RIPCEL, has been developed for the computation of unsteady wave-driven coastal currents. RIPCEL is based on the depth-averaged Navier-Stokes equations. The coefficient of viscosity depends on the local conditions of waterdepth and wave height. As far as the grid generation system is concerned, one set of gridlines should remain straight, while the other set may be curved. For details of the method the reader is referred to [10].

In 1981 RIPCEL has been tested for conditions where analytical solutions are known such as wave set-up, longshore currents and nearshore circulation cells. Furthermore preliminary calculations were made of currents around breakwaters and in a closed basin.
The research described in the present report is directed towards a comparison between RIPCEL and data obtained from laboratory experiments and to determine which of the processes in the equations of motion could be regarded as leading terms in certain parts of the wave basin. One of the topics, which could relatively easily be handled by means of RIPCEL and contains aspects similar to currents around breakwaters is that of wave driven currents in a closed basin. On this topic two more or less complete data sets were available. The first data set has resulted from a few pilot investigations on longshore currents carried out in 1978 at the Delft Hydraulics Laboratory. These tests are reported in [12]. The objectives of these experiments are:

a evaluation of measurement systems;
b differences between current patterns in open and closed basins;
c the outbreaking rip current.

The second data set has been obtained by Mr. P. Visser from the Delft University of Technology during his research programme on wave driven coastal currents. These tests are presented in [9]. Mr. Visser has also contributed to the present study on the topics of bottom friction and lateral mixing.

The present investigation is part of a research programme "Coastal Investigations" sponsored by the Ministry of Transport and Public Works - Rijkswaterstaat in which the Delft Hydraulics Laboratory and the Delft University of Technology participate.

The author, Dr. H.G. Wind, acknowledges many helpful and stimulating discussions with Prof. dr. C.B. Vreugdenhil and the programming efforts of Mr. C. ten Napel.

2. Description of the laboratory data

2.1 Experimental data from the wave basin at the Delft Hydraulics Laboratory (D.H.L.)

The experiments on wave driven coastal currents at the Delft Hydraulics Laboratory have been carried out in the basin shown in Figure 1. The outside dimensions of the basin are 30 m by 30 m. The slope of the concrete beach is 1:50. The horizontal area between the wave generators and the slope is also cast of concrete. The side walls of the basin are plastered.

The still waterdepth d in the basin is 0.264 m. The wave height of the regular waves with a period of 1 s is 0.043 m. The angle between the wave generators and the slope is 20^{o}. From the experiments it followed that the width of the breaker zone was 3.30 m or measured along the y-axis in Figure 1 the width was 3.50 m. The breaker index defined as H/(d) was equal to 0.7. In Figure 2 reference is made to two experiments. In experiment A the longshore current could leave the basin and re-entered the basin at the upstream end. The volume of water which was pumped around in this experiment was chosen such that the circulation in the basin was minimal. In experiment B the current recirculated through the basin and no water was pumped around. Wave height and set-up of both experiments are shown in Figure 2. The data of experiment B will be used to compare with results obtained with RIPCEL. The wave height data for RIPCEL and the resulting set-up are shown in Figure 2 by drawn lines. Details about the experiments A and B can be found in [12]. The wave height, set-up and velocity field relevant for the present study are summarized in Table 2 and Table 3. The Sections I through III are located at 9.37 m, 13.37 m and 17.37 m from the still water line measured parallel to the side wall. The Sections IV and V are located at x = 15.60 , and x = 21.60 m (see Figure 1). The remaining information can be found in the Tables 2 and 3. The test conditions are summarized in Table 1.

2.2 Experimental data from the wave basin at the Delft University of Technology (D.U.T.)

The dimensions of the wave basin at the Delft University of Technology are 15 m by 20 m. The lay-out of the basin is shown in Figure 3. The basin is plastered with concrete. The slope of the beach is 1:10. The oblique incident regular waves are generated with a lamellae type wave generator.

The waterdepth in the horizontal portion of the wave basin is 0.399 m and the waveheight is 0.072 m. The regular waves with a period of 2.01 s approach the plane beach at an angle of 31.1^{o}. The distance between the still-water line and the breakerline measured normal to the shore is 1.06 m. The breaker index $\gamma = H/h$ equals 0.95, where h is the mean water depth (Figure 4).

During the course of the investigation of wave driven longshore currents a large number of experiments have been carried out. The results can be found in [9]. In the present study the data of the experiment in a closed basin will be used. The position of the sections 1 through 5 at the still water line are located at x = 2.55 m, 6.15 m, 9.74 m, 13.34 m and 16.94 m respectively. The position of the sections 6 and 7 along the side walls is at y = 16.68 m and y = 8.38 m respectively. The remaining information is presented in the Tables 4 through 6. Test conditions are summarized in Table 1.

2.3 Evaluation of the laboratory data

The breakertype in the D.U.T. basin was plunging while spilling breaking took place in the D.H.L. basin. This observation correlates with the surf-similarity parameter ξ defined by Battjes (1974) as

$$\xi = \tan\alpha / \sqrt{H/L_o} \qquad (2.3.1)$$

where:

$\tan\alpha$ = beach slope

H = waveheight (m)

L_o = deep water wavelength (m)

In case of D.U.T. experiment this parameter is 0.94 which is in the plunging breaker range, while in the D.H.L. experiments the surf similarity parameter

equals 0.12 which is in the range of spilling breakers.

In their study on bottom frictional stresses and longshore currents due to waves with large angles of incidence, Liu and Dalrymple (1978) show that in order to determine whether a non-linear interaction between waves and currents is relevant two parameters are important: the angle of wave incidence at the breakerline and the ratio of slope steepness m and a frictional parameter f.
The angle of wave incidence at the breakerline in case of the D.H.L. tests is 11^{o}, while in case of the D.U.T. tests this angle is 20.9^{o}. The friction factor f is by definition equal to 8 times the friction factor C mentioned by Longuet Higgins. In the 1970 paper of Longuet Higgins the factor C is estimated to be in the order of 0.01, while James (1972) suggests C = 0,003. This results in the following values of m/f.

	m/f for a slope 1:10	m/f for a slope 1:50
C = 0.01	1.25	0.25
C = 0.003	4.17	0.83

Taking into account the angle of wave incidence, then it follows from the theory of Liu and Dalrymple (1978) that the conditions in case of the D.U.T. tests are that of strong currents requiring a non-linear interaction between waves and currents as far as bottom friction is concerned. The value of 0.25 m in case of the D.H.L. tests is in the weak current range, while the value of 0.83 is in the intermediate range.
This evaluation suggests that from the point of view of bottom friction the D.H.L. experiment will be easier to model than the D.U.T. experiment.

3. Choice of numerical parameters

3.1 Introduction

For the calculations a choice has to be made for the following parameters:

a gridsize Δx
b timestep Δt
c weighing coefficient Θ in the difference scheme.

In [10] the conditions for these parameters are formulated. These will briefly be repeated here. The grid size determines the resolution of flow details. Reduction of the grid size will reveal more detail of the flow, but the number of grid points and hence computation time will increase. However, if in an area of large velocity gradients the gridsize is too large, then the flow may seriously be distorted. An important parameter for this aspect is the cell Reynolds number $R_{\Delta x}$

$$R_{\Delta x} = \frac{U\ \Delta x}{\varepsilon} \tag{3.1.1}$$

where:
U = velocity scale
ε = viscosity
Δx = characteristic length

In the region of large velocity gradients the cell Reynolds number should be smaller than 2.

The stability condition for the numerical scheme is:

$$\Theta \geq \tfrac{1}{2} \tag{3.1.2}$$

A condition for the Courant number

$$C_r = \frac{c\ \Delta t}{\Delta x} \tag{3.1.3}$$

where c is the velocity of wave propagation, does not exist for the implicit scheme.

Due to truncation errors in the numerical representation of the differential equation an additional effect is generated named numerical viscosity. In

[10] the order of magnitude of the numerical viscosity is estimated to be:

$$\varepsilon_{num} \simeq (\Theta - \tfrac{1}{2}) \quad \Delta t \; gh \tag{3.1.4}$$

3.2 The gridsize

For the condition (3.1.1) on the gridsize Δx an estimate of the viscosity is required. In his 1970 paper Longuet-Higgins presents the following estimate of ε

$$\varepsilon = N \; |y| \; (gh)^{\frac{1}{2}} \tag{3.2.1}$$

Although in recent literature also other relations for ε are suggested, it is expected that (3.2.1) will be sufficiently accurate for the order of magnitude estimate of Δx. From (3.2.1) and (3.1.1) follows that

$$\Delta x \leqslant 2N \; gh^{3/2}/(Um) \tag{3.2.2}$$

where use has been made of the relation $h = ym$ where m is the beach slope. An area of large velocity gradients is located in the outbreaking rip current. In that area the velocity U is less than 0.2 m/s and the waterdepth is at least 0.1 m. For a value of $N = 0.016$ [6] and a beach slope $m = 0.02$ Δx should according to (3.2.2) be smaller than 2.50 m. For similar conditions on a slope $m = 0.1$ this dimension is 0.50 m. In the area of the outbreaking rip current the gridsize will be smaller than follows from (3.2.2). It is therefore not to be expected that the cell Reynolds condition will cause important inaccuracies.

3.3 The time step Δt and Θ

The time step Δt and Θ determine the magnitude of the numerical viscosity (3.1.4). A requirement could be that throughout the solution area

$$\frac{\varepsilon_{num}}{\varepsilon_{phys}} \leqslant a \tag{3.3.1}$$

where a is a constant, e.g. 0.1. Combining (3.2.1) and (3.1.4) yields

$$\Delta t \leqslant a \frac{N h^{\frac{1}{2}}}{(\Theta-\frac{1}{2}) m g^{\frac{1}{2}}} \qquad (3.3.2)$$

In the area near the shoreline the time step Δt should go to zero according to (3.3.2). In the middle of the breakerzone at a depth of 0.05 m and Θ = 0.53 the time step is $\Delta t \leqslant 0.12$ s for a slope of 1:50 and $\Delta t \leqslant 0.023$ s for a slope of 1:10. Outside the breakerzone at a depth of 0.30 m these values are 0.29 s and 0.058 s respectively. The value of a in (3.3.1) has been assumed to be 0.1

The value of θ has not been chosen smaller than 0.53 because stability problems were feared from (3.1.2). For a final choice of Δt and Θ an experimental verification has been carried out.

3.4 Experimental verification

In order to verify the estimates made in paragraph 3.1 through 3.3 a preliminary set of calculations have been carried out using the conditions in the D.U.T. basin because these conditions are more severe than the conditions for the D.H.L. basin. In these calculations expressions for bottom friction and lateral mixing as suggested by Longuet Higgins (1970) have been used.

In order to determine the time required to reach an equilibrium condition the time function of the velocity of a point inside the breakerzone in section III and in section VII have been plotted in Figure 5. From this figure follows that an equilibrium state is attained after 30 s. Next the following set of calculations have been carried out.

test number	Θ	Δt
A	0.55	0.5
B	0.53	0.5
C	0.53	1.0
D	0.53	0.1

In addition to the points mentioned above the time function of a point in section VI has been plotted in Figure 6 for the conditions A through D summarized in the table.

The conclusions from Figure 6 are:

a the reduction of Θ from 0.55 to 0.53 has a marginal effect
b the increase in time step from 0.5 s to 1.0 s yields an unstable condition
c the reduction in time step from 0.5 s to 0.1 s yields a change in velocity in the low velocity area.

It appears that the effect of numerical viscosity in condition B is small relative to the physical viscosity. Furthermore does the condition B lead to a stable solution. For the remaining calculations the combination of Θ and Δt mentioned for condition B will be applied.

4. Numerical modeling of the D.H.L. basin

4.1 Introduction

For the numerical modeling of the D.H.L. basin a choice has to be made for the description to be used for the following processes.

a wave refraction and shoaling
b position of the breakerline
c energy dissipation inside the breakerzone
d wave current interaction
e bottom friction
f lateral mixing

In the literature various descriptions can be found for most of the processes mentioned above. In case of energy dissipation inside the breakerzone this concerns mainly empirical data, while for instance in case of bottom friction in relation to the present wave and current field theoretical models have been developed [5]. It is clearly out of the scope of the present study to compare all possible interesting combinations of a) through f) with the available data. In the present study the following approach has been chosen. For each of the processes a) through f) an approximation will be used similar to that applied by Longuet Higgins in case of longshore currents on an infinitely long straight beach. On basis of the resulting current pattern further improvements can be made.

4.2 The wavefield

In his paper of 1972 Longuet Higgins shows that the waves outside the breaker-zone exert a lateral thrust on the water and sediment inside the surf zone. A prerequisite for a numerical modelling of the wave driven longshore current is that the longshore thrust is properly represented. Longuet Higgins presents the following relation between longshore thrust S_{xy} and energy flux towards the shore F_x

$$S_{xy} = \frac{\sin \phi}{c} F_x \qquad (4.2.1)$$

The energy flux towards the shore is defined as

$$F_x = E\, c_g \cos \phi \qquad (4.2.2)$$

E = local energy density
c_g = group velocity
ϕ = angle between wave crest and depth contour

The resulting average width of the breakerzone has also been applied in the numerical model. The breaker index γ defined as

$$\gamma_b = H_{num(b)}/h_b \qquad (4.2.3)$$

$H_{num(b)}$ = calculated wave height at the breakerline
h_b = still water depth at the breakerline

has been used to calculate the waveheight distribution inside the breakerzone. A comparison between the calculated- and observed waveheight distribution is shown in Figure 2. It follows from Figure 2 that inside the breakerzone the observed wave height is lower than the calculated waveheight. This may point towards the fact that the distribution of the longshore thrust over the breakerzone in the numerical model and laboratory experiment is different in both cases. For a more definite statement on this point the actual flux of momentum of the breaking waves should be considered (Stive and Wind, 1981).

The relation 4.2.1 does not depend on application of small amplitude wave theory. If the following conditions are satisfied outside the breakerzone:

a no reflection
b no wave current interaction
c no dissipation of energy

then the energy flux towards the shore is conserved. This means that the energy flux towards the shore can be modeled in deep water and that the energy is transported towards the shore with 4.2.2. resulting in the required longshore thrust S_{xy}. In deep water the local energy density of the waves can be approximated as

$$E = \frac{1}{8} \rho \, g \, H_{r_{ms}}^2 \qquad (4.2.4)$$

In the laboratory experiment the value of $H_{r_{ms}}$ has been determined.

In the calculation of the direction of wave propagation the effect of wave current interaction initially will be neglected and Snells law will be applied.

The position of the breakerline has been determined in the laboratory experiment.

4.3 Bottom friction and lateral mixing

The bottom friction in case of weak currents and almost normally incident waves has been derived by Longuet Higgins (1970) as

$$\tau_{Bx} = \frac{2}{\pi} \rho \, C \, U \, u_{max} \qquad (4.3.1)$$

C = friction coefficient

U = longshore current velocity

u_{max} = maximum orbital velocity of the waves at the bottom

The maximum orbital velocity of the waves has been approximated inside and outside the breakerzone by Longuet Higgins as:

$$u_{max} = \tfrac{1}{2} \gamma \sqrt{gh} \qquad (4.3.2)$$

In the numerical approach the set-up η is initially unknown. In first approximation therefore 4.3.2 has been reduced inside the breakerzone to

$$u_{max} = \tfrac{1}{2} \gamma \sqrt{gd} \qquad (4.3.3)$$

and outside the breakerzone to

$$u_{max} = \tfrac{1}{2} \frac{H}{d} \sqrt{gd} \qquad (4.3.4)$$

The longshore current velocity U in 4.3.1 has been replaced by the component of the velocity in x direction.

In his paper of 1970 Iwata shows that in the present approximation the bottom

friction is essentially anisotropic, the bottomfriction coefficient in the direction of wave propagation being twice as large as in the direction parallel to the wave crest. This point has been taken into account by assuming that

$$\tau_{By} = \frac{4}{\pi} \rho \, C \, V \, u_{max} \qquad (4.3.5)$$

The eddy viscosity coefficient has been approximated as

$$\varepsilon = N \, r \, \sqrt{gd} \qquad (4.3.6)$$

N = constant
r = distance normal to the shore

In the analytical approximation Longuet-Higgins assumes the relation 4.3.6 both inside and outside the breakerzone. In the numerical approximation the eddy viscosity coefficient in the area outside the breakerzone will be kept at the value attained by 4.3.6 at the breakerline. Inside the breakerzone 4.3.6 will be used.

In [6] estimates of C are ranging between 0.034 and 0.097 for the description of damping of sea waves over a smooth, level and impermeable seabed. Analysis of laboratory experiments of Miller in [6] yields values of C between 0.01 and 0.02. In his study on non-linear wave forcing of longshore currents James (1972) finds C values in the order of 0.0025. In the literature several reasons are mentioned why differences in C values are to be expected. However there is no uniquely defined relation for C available. Therefore C will be used as a fit parameter. As far as N is concerned it is expected [6] not to exceed 0.016.

In his study on longshore currents Longuet Higgins has represented the relative importance of lateral mixing to bottom friction in the parameter P

$$P = \frac{m \, N}{\gamma \, C}$$

where m is the beach slope and γ is the breaker index. In the same paper it is shown that the relative position of the maximum longshore current velocity is a function of P only. The magnitude of the maximum velocity is among others a function of P and C. This means that from the shape of the longshore current

distribution and of the observed maximum current velocity estimates of N and C can be obtained for a given geometry and wavefield. Translating these values for a infinite long straight beach to a closed basin will show differences because of the interaction between the circulation and the longshore current.

For the D.H.L. test the value of C has been estimated at 0.003 and N at 0.01. The resulting P value is 0.095.

4.4 Calculation of the current field in the D.H.L. basin

On basis of the information provided in the previous paragraphs a calculation of the current pattern can be made. In Figures 7 and 8 the resulting current patterns after respectively 32 s and 56 s are shown. In Figure 7 an offshore oscillation in the current field can be noticed. This initial oscillation is damped out after 56 s as shown in Figure 8.
A first impression of the current field in Figure 8 is that the order of magnitude of the longshore current is right, but the velocities in the outbreaking ripcurrent are an order of magnitude too low. A second aspect is that the centre of recirculating flow is located near the breakerline, while in case of the observations this centre was located in a more offshore position. In order to check once more the numerical routine it was decided to make the following calculation

a rectangular basin
b oblique incident waves
c no wave shoaling

The effect of the rectangular basin is that most of grid transformation terms are zero. A point added to b is that the waves are running through the side walls. Diffraction is absent. The effect of excluding wave shoaling on the gently sloping beach (1:50) is that gradients in the wave action in the shoaling region are zero. The resulting current pattern is shown in Figure 9. It will be clear that the phenomena in Figures 8 and 9 are similar. It was therefore decided that at present there is no reason to doubt the numerical programme which has been carefully checked otherwise on previous occasions, and to accept the resulting current pattern in Figure 8 as a good approximation of the exact solution of the mathematical system.

The longshore current distribution both in longshore and in offshore direction as obtained in Figure 8 is presented in Figure 10. In this figure also the experimental data is presented. The laboratory data is insufficient for a proper evaluation. The current distribution in offshore direction shows similar tendencies as observed in the laboratory. It is important to note that the numerical offshore current distribution drops off faster than the observed current distribution. This difference points towards an eddy which is present in the laboratory set-up, but not (yet?) in the numerical model. The eddy in the laboratory experiments is rather important for the outbreaking ripcurrent. The point can be explained by comparing the volume of the longshore current between the shoreline and the breakerline with the volume of the ripcurrent in the laboratory experiments.

	volume of longshore current (m^3/s)	volume of ripcurrent (m^3/s)
D.H.L.	0.010	0.040 (Section III)
D.U.T.	0.028	0.082 (Section VII)

In both experiments the discharge of the ripcurrent is several times larger than the discharge of the longshore current. Part of this increase in discharge of the ripcurrent will be provided by the "tail" of the longshore current while another part results from the circulation in the basin.

It follows from Figure 8 that the observed volume of the ripcurrent is not present in the calculated current pattern, resulting in low velocities along the sidewalls. The observed high velocities along the sidewalls, caused by the interaction between longshore current and nearshore circulation are especially relevant for sediment transport. It is seen from the results in Figure 8 and Figure 10 that the proper tendencies of the longshore current are present, but that the choice of the parameters is not yet optimal. The calculated nearshore current pattern outside the breakerzone shows significant differences with the observed current field. Various causes for these differences will be discussed in the following chapters. However before entering into an optimizing stage it seems useful first to analyse the available numerical data and to carry out some theoretical analyses of the phenomena involved.
Finally, it may be remarked that the current patterns for the D.U.T. basin are shown in Figures 16 and 17. The tendencies are similar to those of the D.H.L. and hence will not be discussed independently in this report.

4.5 Analysis of the numerical data

4.5.1 Introduction

The numerical data concerns the value of p, q and h in each of the 483 grid-points. Furthermore quantities such as time derivative, convective terms, viscosity terms, pressure term, bottom friction terms and gradients in wave action are also interesting. This yields a total of 7245 numbers in each timestep. In order to present this wealth of information in a systematic fashion the numbers have been reduced to the following forms

a the magnitude of the terms in the p and q equation in 16 selected points
b the relative importance of the terms in the p and q equation in 90 points.

4.5.2 The magnitude of the terms in the p- and q-equation in selected points

In Figure 8 16 points are selected for further investigation. The points are numbered with K running in longshore direction and J in offshore direction. Points with J = 4 are located near the maximum velocity in the longshore current, while J = 8 is situated just outside the breaker zone. The points with J = 12 and J = 16 are located in the offshore circulation system. The outbreaking ripcurrent contains points with K = 20. The magnitude of the terms in the p and q equation in the selected points are presented in Tables 7 and 8. The definition of the terms can be found in appendix A, with the exception of the time derivative. The time derivative has been calculated in this case such that the total sum of all the terms in the relevant equation should equate to zero. Three aspects should be noted from Table 7 and Table 8. The first aspect is that in most cases the wave pressure gradient is balanced by the pressure gradient due to the change in mean water level. The second point is that of the remaining terms the time derivative is not an order of magnitude smaller than for instance the viscosity terms or the convective terms. Finally does the time derivative change of sign for lines parallel to the shoreline (constant J). The magnitude of $\frac{\partial p}{\partial t}$ or $\frac{\partial q}{\partial t}$ is 10^{-4} m^2/s^2. For a uniform waterdepth of 0.20 m this implies that $\frac{\partial u}{\partial t}$ and $\frac{\partial v}{\partial t}$ are in the order of 5.10^{-4} m/s^2. This means that for a change of u and v of 10^{-2} m/s a period of 500 s. is required. From this point of view one might state that the current pattern in Figure 8 is stationary. However if the magnitude of the convection, viscosity and bottom friction

terms are compared with the time derivative then a significant change of the current pattern should be envisaged, except if the time derivative is finally balanced by a surface pressure gradient similar as in case of a long wave. According to Table 7 the longshore current (J = 4) is accelerating in the intermediate part (K = 8 and K = 14) and decelerating at the inflow and outflow area (K = 2 and K = 20). This shows that a definite conclusion about changes of the current field with increase of time is hard to predict from the Tables 7 and 8. Comparing the Figures 7 and 8 then the shape of the current pattern remains conserved while the changes between T = 32 s and T = 56 s are much smaller than between T = 0 and T = 32 s pointing towards reaching an equilibrium current pattern. It should be remarked that the definition of time derivative used in this paragraph differs from the definition used in RIPCEL. This may influence the conclusions somewhat.
Next the magnitude of terms of the equations of motion relative to the wave pressure gradient will be studied in more points than in the present paragraph.

4.5.3 The relative importance of the terms in the p and q equation in 90 points

Wave driven currents are generated by wave action. A useful parameter for the relative importance of the various terms in the equation of motion therefore seems to be the gradient in wave action. The lines with J = constant are running more or less parallel to the shoreline and because current refraction has been neglected the gradients in wave action should be comparable along lines with J = constant. This point can be verified in Table 7 and 8. The selected points in this paragraph are points with even values for J and K.
In the tables 9 through 18 the ratio of the various terms and the gradient in wave action can be found.
The time derivative can be found in Table 9 and Table 14. Especially in Table 9 can be seen that the time derivative changes of sign for constant J, pointing towards an oscillation around an equilibrium stage.
In Table 13 and Table 18 the pressure head is presented. The ratio between the gradient in wave action and the pressure gradient is in the order of 100%. This means that as a first approximation the gradients in wave action are balanced by gradients in mean water level. This is in line with the proof presented by Battjes (1974) that outside the breakerzone no currents are driven by a variation in wave height except if this variation is caused by wave breaking. In Tables 13 and 18 both in offshore and in longshore direction

minor undulations can be distinghuised. Although these undulations follow from minor irregularities in the mean waterlevel of 10^{-4} m it should be remarked that these irregularities effect the pressure head at least in the order of 20% and this is according to Table 7 and 8 also the order of magnitude of say the convective terms. This point requires further attention at a later stage of the research.
A consequence of these minor irregularities at the present stage of the research is, that the numerical data should be analysed more in a broad than in a detailed fashion.

It follows from Table 10 and 15 that the convection terms are mainly dominant in the outbreaking ripcurrent. To some extent at the inflow side of the ripcurrent parallel to the shoreline also the effect of convective terms can be noted, however it should be remarked that the free slip condition has been applied between J = 1 and J = 2. This point may influence to some extent the results parallel to the shoreline. The free slip zone can also be noticed in Figure 10. The bottomfriction terms presented in Tables 12 and 17 dominate the viscous terms shown in Tables 11 and 16 in the longshore current parallel to the shoreline. Just outside the breakerline (J = 7) the viscous terms take over and are much larger than the two friction terms in the large scale circulation outside the breakerzone.

A qualitative impression about the importance of the various terms, can be obtained if the calculations leading to the current pattern at T = 32 s in Figure 7 are repeated, but now excluding one of the factors convection, viscosity or bottom friction. In Figure 12 the current pattern is presented but excluding the convective terms. A comparison between Figure 7 and Figure 12 shows that they are almost indistinguishable. In Figure 13 the bottomfriction terms have been set to zero. The flow is now governed by viscous and convection terms. A comparison between Figure 7 and Figure 13 learns that large scale features remain essentially unchanged, while the magnitude of the longshore velocities has increased somewhat. Finally Figure 14 shows the current pattern with the viscosity terms excluded. This change seems, according to Figure 7, to have induced the relative largest changes. At the inflow side of the longshore current the whole pattern changes. The longshore current distribution becomes more triangular as follows from the theory on longshore currents. Downstream of the longshore current the pattern becomes rather disordered.

The conclusion of the patterns in Figure 12 through 14 is that all the terms are more or less of the same importance. For the present low velocity case the convective terms only marginally affect the current pattern. The viscosity terms and the bottomfriction terms seem to play an interchangable role for the overall circulation pattern. On details the effects of viscosity and bottomfriction terms are different.
None of the calculations presented in the Figures 12 through 14 show a significant improvement in the representation of the outbreaking ripcurrent. In line with these experiments it is not expected that by using a different theory for bottomfriction or lateral mixing an improvement on this point will be achieved.

4.5.4 Conclusions

In Tables 7 and 8 the magnitudes of the various terms in the equations of motion are presented. From these tables the following conclusions can be drawn.

- The time derivative is in the order of 10^{-4} m/s, pointing towards an equilibrium state.
- The time derivative is not small relative to the convective, viscous or bottom friction terms.
- If a minor long wave oscillation is present, then the time derivative is balanced by a gradient in the mean water level.
- The gradient in wave action is balanced to a large extent by the pressure head e.g. set-up and set-down.

In Tables 13 and 18 the percentage of the gradient in wave action which is balanced by wave setup is presented. Following lines of constant values of J minor oscillations in the watersurface elevation, in the order of 10^{-4} m, can be noticed. This "noise" however is in the present weak current case of the same order of magnitude as the current dominating terms.
In the present example the individual effect of the convective, viscous, bottomfriction and lateral mixing terms on the current pattern is rather indistinguishable.

In Tables 10 through 12 and 15 through 17 the convection, viscous and bottomfriction terms are presented. It follows that

- convective terms are mainly important at in- and outflow of the longshore current

- bottomfriction exceeds viscosity in the near shore region

- viscous terms exceed the bottomfriction terms in the eddy

These conclusions are verified in a series of numerical tests presented in Figures 12 through 14. These figures should be compared with Figure 7. In all Figures the large scale phenomena are reasonably represented, the viscosity terms and bottomfriction terms playing an interchangeable role. For the modelling of the rip current an interaction between longshore current, eddy and outbreaking rip current is required. However this interaction has not yet been established in the numerical model. The cause of this interaction is not clear. One might think about 3-D effects, wave current interaction or turbulence modeling.

5. Onset to a theoretical analysis

5.1 Introduction

In the study of wave driven coastal currents and related circulations various topics regularly came forward. Examples of these topics are:

- the driving mechanisms
- convergence or divergence of streamlines
- vorticity
- velocity field in the viscous circulation flow
- time scales in the current pattern in the basin.

In this paragraph a theory will be presented which is related to these topics. The results in the paragraph are not all in a final stage and are meant to stimulate discussion on the topics mentioned above.

5.2 The physical mechanisms

For an analysis of the differences between the calculated and observed current pattern in Figure 8, it is important to specify clearly the various driving mechanisms.
As far as waves are concerned Battjes (1974) proves that a steady distribution of wave action in irrotational waves is equivalent to a steady distribution of normal pressures at the water surface, and should give rise to (spatial) variations in the surface elevation only, without driving a mean current. This can be expressed as

$$\frac{\partial}{\partial x} S_{xx} + \frac{\partial}{\partial y} S_{xy} + \rho g h \left(\frac{\partial h}{\partial x} + \frac{\partial z_b}{\partial x}\right) = 0 \qquad (5.2.1)$$

$$\frac{\partial}{\partial y} S_{yy} + \frac{\partial}{\partial x} S_{xy} + \rho g h \left(\frac{\partial h}{\partial y} + \frac{\partial z_b}{\partial y}\right) = 0 \qquad (5.2.2)$$

If a current is driven by other sources then this may lead to changes in the gradient in mean water level. However these changes will be balanced by viscous bottomfriction or convective effects.
Inside the breakerzone the waves are generating a driving force. This force is balanced by

a viscosity
b bottom friction
c convection
d gradient in mean water level.

From the Tables 9 through 18 it follows that inside the breakerzone the set-up and gradient in wave action are largely balanced. The remaining imbalance between gradient in wave action and set-up is driving the longshore current. An impression of the magnitude of the driving force of the longshore current S_{xy} relative to the force balancing the wave set-up system up S_{yy} can be obtained in case of an infinite straight beach. At the breakerline the ratio of S_{xy} over S_{yy} is according to linear theory

$$S_{xy}/S_{yy} = \sin 2\Theta/(2\cos^2\Theta+1) \qquad (5.2.3)$$

or in tabulated form

Θ	S_{xy}/S_{yy}
0^o	0
10^o	0.116
20^o	0.232

This means that the force driving the longshore current is only a small portion of the force balancing the wave set-up.

It follows from Tables 10 and 15 that the convection terms are small far away from the sidewalls. The viscosity term becomes important near the breakerline and is comparable with the bottom friction term. Summarizing it follows that the driving force of the longshore current is largely balanced by bottom friction and lateral mixing.
Driving mechanisms for the rip current are:

a gradient in mean water level caused by retardation of the longshore current,
b entrainment of mass from the eddy
c viscosity between current and eddy
d bottom friction.

A parameter for the streamline pattern is the vorticity. The relation between streamline pattern and vorticity will be treated in paragraph 5.3.
Driving mechanisms for the eddy are

a lateral friction between longshore current and eddy
b lateral friction between rip current and eddy
c bottom friction.

Observations in the model indicate that the centre of the eddy is located much further offshore than is the case in the numerical model and that the rip current extracts much more mass from the eddy than follows from the calculated flow field. A first hypothesis could be that the driving force of the eddy, lateral mixing, is not properly represented. Further suggestions could be 3-D effects and wave current interaction. The 3-D effects did not clearly appear from the measurements which showed a more or less uniform velocity distribution over the depth in the current. Wave current interaction may not be the determining factor because observations have been made of narrowing of offshore currents near structures in absence of waves.
Because of the differences between observed and calculated velocity distribution in the eddy it is expected that the interaction between longshore current and eddy is not properly represented in the numerical model. This implies that the choice of the bottom friction coefficient may also be erroneous, because that choice was based on a reproduction of the maximum longshore current velocity.

5.3 Convergence or divergence of streamlines; vorticity

In the numerical model (Figure 8) the streamlines of the rip current are diverging much stronger than is the case in the observations. Convergence or divergence of streamlines is closely related to vorticity. This relation becomes clear if the equations of motion are reduced to the vorticity transport equation. In Appendix C the derivation of this formula can be found.
Vorticity is defined as the anti-clockwise rotation of the diagonal of a fluid element.

$$\omega = \frac{\partial u}{\partial y} - \frac{\partial v}{\partial x} \tag{5.3.1}$$

In textbooks it is shown that internal friction is a prerequisite for the generation of vorticity. If vorticity is absent then the class of fluid flows is reduced to potential flow satisfying

$$\frac{\partial h}{\partial t} + \frac{\partial \phi}{\partial x}\frac{\partial h}{\partial x} + \frac{\partial \phi}{\partial y}\frac{\partial h}{\partial y} + h\left(\frac{\partial^2 \phi}{\partial x} + \frac{\partial^2 \phi}{\partial y^2}\right) = 0 \tag{5.3.2}$$

where

$$u = \frac{\partial \phi}{\partial x} \quad \text{and} \quad v = \frac{\partial \phi}{\partial y} \tag{5.3.3}$$

If the fluid at infinity remains at rest, and the initial conditions are that u and v are zero and h is constant, then it follows from (5.3.2) that the fluid flow remains at rest. If vorticity is present then inside the breakerzone the vorticity generation is described by Eq. (C.9) and outside the breakerzone by Eq. (C.12). It follows from (C.9) that vorticity is generated by the wave action terms, transported by the convective terms and dissipated by the bottom friction and viscous terms. In principle the viscous terms as well as friction terms can generate vorticity near a wall, but because of the free slip conditions this possibility is excluded. The transport of vorticity and dissipation of vorticity will be studied for the following condition. Consider a rip current normal to a plane beach. The fluid motion is stationary and viscous effects will be neglected. The vorticity transport equation is in this case according to (C.23):

$$\frac{\partial}{\partial s}\left(\frac{\omega}{h}\right) + \left(\frac{\omega}{h}\right)\left\{\tfrac{1}{2}C\,\frac{H}{h}\,\frac{(gh)^{\frac{1}{2}}}{Uh}\right\} = 0 \tag{5.3.4}$$

In his study on dynamics of rip currents Arthur (1962) neglects bottom friction. He finds the relation:

$$\frac{\partial}{\partial s}\left(\frac{\omega}{h}\right) = 0 \tag{5.3.5}$$

or

$$\frac{\omega}{h} = C_1 \tag{5.3.6}$$

This means that the vorticity per unit depth is conserved along a streamline.

From the definition of vorticity and of the stream function the following relation can be obtained

$$h\omega = - \nabla^2\psi + U \frac{\partial h}{\partial n} \qquad (5.3.7)$$

For the example of a rip current on a plane beach $\frac{\partial h}{\partial n} \simeq 0$ near the centre-line and the longshore gradient in the offshore discharge will be much larger than the offshore gradient in the longshore discharge ($\frac{\partial^2\psi}{\partial y^2} << \frac{\partial^2\psi}{\partial x^2}$). Equation (5.3.7) reduces under these conditions to

$$h\omega = - \frac{\partial^2\psi}{\partial x^2} \qquad (5.3.8)$$

With (5.3.6), (5.3.8) can be written as

$$C_1 = - \frac{1}{h^2} \frac{\partial^2\psi}{\partial x^2} \qquad (5.3.9)$$

This implies that with increasing depth, $\frac{\partial^2\psi}{\partial x^2}$ also increases and vice versa. An increase in $\frac{\partial^2\psi}{\partial x^2}$ means convergence of the streamlines. Arthur uses this mechanism as an explanation for the current pattern of a rip current. The effect of bottom friction on this current pattern follows from integration of (5.3.4). Assume that the beach slope is constant or

$$h = m.s \qquad (5.3.10)$$

and that the vorticity per unit depth is ω_o/h_o at S_1. The solution of (5.3.4) is

$$(\frac{\omega}{h}) = \frac{\omega_o}{h_o} \, e^{- C \frac{H}{p} (\frac{g}{m})^{\frac{1}{2}} (S_1^{\frac{1}{2}} - S^{\frac{1}{2}})} \qquad (5.3.11)$$

where $p = U.h$ is constant along the streamlines. The initial value of ω_o/h_o has been reduced to a fraction of e^{-1} of the original value over a relative distance of S/S_1 of

$$S/S_1 = \left\{ 1 - 1/(C \frac{H}{h} \frac{(gh_b)^{\frac{1}{2}}}{U}) \right\}^2 \qquad (5.3.12)$$

In the present test conditions: $U \simeq 10^{-1}$ m/s, $h = 10^{-1}$ m, $C = 10^{-2}$, $H = 5.10^{-2}$ m or the relative dissipation distance is 80. This means that bottom friction does not seriously reduce the observed phenomenon of convergence of stream-

lines. For prototype conditions S/S_1 should be compared with the width of the breakerzone. The estimate of p is rather crucial for a final conclusion. This extension will not be treated in this report.

Tam (1973) has studied rip currents in terms of the flow in a two-dimensional incompressible jet. He finds that the velocity in offshore direction should change inversely proportional to the distance offshore, so the product of offshore velocity and offshore distance is constant. The observations in D.H.L. basin are shown below.

Offshore distance y (m)	Velocity v (m/s)
9.37	0.14
13.37	0.12
17.37	0.10

From this table follows that the velocity in offshore direction does not drop off as fast as should be expected from the theory. This may mean that the entrainment rate of fluid from the circulation into the rip current is larger than predicted. It has been noticed in paragraph 4.4 that the discharge of the rip current has increased with a factor 3 to 4 in offshore direction.

5.4 Velocity field in the viscous circulation flow

The large scale circulation in the area outside the breakerzone could approximately be regarded as a viscous fluid motion, driven along the sides by the constant velocity gradient and retarded by bottom friction. The equation for the fluid motion has been derived in Appendix D. The resulting equation (D.10) has as a solution a Bessel function

$$y = A\, I_1(z) + B\, K_1(z) \qquad (5.4.1)$$

where I_1 and K_1 are modified Bessel functions of the first kind and of the first order. The boundary conditions for this problem are that the radial velocity is zero

$$u_r = 0 \qquad (r=0) \qquad (5.4.2)$$

and that the tangential velocity u_Θ has a prescribed velocity if r = R.

$$u_\Theta = u_o \qquad (r=R) \qquad (5.4.3)$$

By definition D8, the tangential velocity at a distance r is given by

$$u_\Theta/u_o = y \qquad (5.4.4)$$

and the relation between z and r is given by D7 as

$$z = r(c/\nu)^{\frac{1}{2}} \qquad (5.4.5)$$

The values of I_1 and K_1 can be found in handbooks. The function K_1 shows a pole for z = 0. From the condition (5.4.3) follows that B = 0 in equation (5.4.1). The value of A in (5.4.1) follows from (5.4.3) and (5.4.4). Before calculating the velocity distribution for various values of (c/ν) first the velocity distribution in absence of bottom friction will be derived. If c = 0, then (D.5) can be written as:

$$\nu \left\{ \frac{1}{r} \frac{\partial}{\partial r} \left(r \frac{\partial u_\Theta}{\partial r} \right) - \frac{u_\Theta}{r^2} \right\} = 0 \qquad (5.4.6)$$

or

$$\frac{\nu}{r^2} \frac{d}{dr} \left\{ r^2 \left(\frac{du_\Theta}{dr} - \frac{u_\Theta}{r} \right) \right\} = 0 \qquad (5.4.7)$$

The solution of (5.4.7) is the well-known linear velocity distribution (rigid body rotation)

$$u_\Theta = r.\text{constant} \qquad (5.4.8)$$

In Figure 15 the velocity distribution in a circular basin is presented. The velocity parallel to sidewall is u_o. The parameter c/ν takes values of 0, 0.01, 0.1 and 1.

If the rip current in Figure 10 is caused by the mechanism described in the present paragraph, then according to Figure 15 the bottom friction

outside the breakerzone should be much larger than the value used for the calculations in Figure 10. However, as is shown in paragraph 5.3 an increase in bottom friction would also lead to divergence of the streamlines. The conclusion of this analysis is that two elements of the formation of the rip current have been made clear, but that these elements do not completely explain the observed rip current.

5.5 Time scales in the current pattern in the basin

In the calculation of the current field for wave driven coastal currents various time scales play a role. The time scale of the turbulence and of short waves have been averaged out resulting in an eddy viscosity coefficient and wave action respectively. In Figure 5 small fluctuations in the current velocity can be noticed pointing towards long waves which are generated by sudden application of the wave action. Two more time scales are those related to the build-up of the longshore current velocity and of the circulation in the basin. The time scale for the longshore current will be estimated by assuming a constant waterdepth h, a width of the breaker zone B and a resulting driving force S_{xy}. It follows from Eq. (C.2) after integration over the width of the breakerzone and neglecting viscosity that

$$\frac{\partial u}{\partial t} + C \left|u_{orb}\right| \frac{u}{h} + \frac{1}{Bh\rho} S_{xy} = 0 \qquad (5.5.1)$$

The solution of (5.5.1) is

$$u = - \frac{F_x}{\rho C \left|u_{orb}\right|} \left\{1 - e^{-C \left|u_{orb}\right| \frac{t}{h}}\right\} \qquad (5.5.2)$$

The time required for the build-up of the longshore current follows from the exponent of e. Approximating $\left|u_{orb}\right|$ with the shallow water approximation, then it follows from (5.5.2) that the longshore current has attained a velocity equal to $(1 - e^{-1})$ * maximum velocity after

$$t = \frac{2}{C} \frac{h}{H} \frac{h}{\sqrt{gh}} \qquad (5.5.3)$$

For a waterdepth and waveheight of 0.05 m and C = 0.01 this time is 14 s. This is in agreement with Figure 5.

For the time scale of the circulation in the basin a rigid body rotation

will be assumed, driven by a shear stress τ_ℓ along one half of the outer circle. The waterdepth h is constant. The inertia of the rigid body is equal to $\frac{\pi}{2}$ h R^4. A linear bottom friction law will be applied. The equation of motion now becomes

$$\frac{\pi}{2} h R^4 \frac{d\omega}{dt} + \frac{\pi}{2} C |u_{orb}| R^4 \omega + 2\pi \tau_\ell h R^2/\rho = 0 \qquad (5.5.2)$$

where ω is the angular velocity. Introducing in (5.5.2) $v = \omega R$ and rearranging yields

$$\frac{dv}{dt} = \frac{C}{h} |u_{orb}| v + 2\tau_\ell/(\rho R) = 0 \qquad (5.5.3)$$

The solution of (5.5.3) is

$$v = - \frac{2\tau_\ell h}{\rho C |u_{orb}| R} e^{- C |u_{orb}| \frac{t}{h}} \qquad (5.5.4)$$

It is clear from a comparison between (5.5.2) and (5.5.4) that the time scale of the velocity in the longshore current and of the large scale circulation is the same. This is as one would expect if bottom friction is the cause of the retardation in both examples. The second example has been derived for sake of clarity.

Experience learns that the large scale circulation has a much larger time scale than the longshore current. This could be caused by viscous effects which have not been taken into account in the present analysis. This effect has been studied in [11]. The conclusion of [11] is that the relaxation time of the viscous fluid flow including bottom friction is several times larger than the relaxation time due to bottom friction alone in the present case this means that after say 60 s in the order 70% of the equilibrium velocity distribution has been attained. This implies that the velocity distribution in Figure 10 will only marginally change with the increase of time.

6. Conclusions and recommendations

Choice of numerical parameters

- The timestep is largely determined by the requirement that the numerical viscosity should be smaller than the physical viscosity.

- The choice in the present calculations of the timestep Δt, and the weighing coefficient in the difference scheme Θ is such that the effects of numerical viscosity can be discarded.

Numerical modelling of the D.H.L. basin

- The calculated longshore current distribution shows similar tendencies as the observed velocity distribution both in longshore and offshore direction.

- The range of known values of bottom friction and viscosity coefficient is such that a close agreement between observed and calculated longshore current velocity distribution can be obtained.

- The calculated velocities in the rip current are much smaller than the observed velocities.

- In the present analysis the time derivative is very small after 56 s, but this term is not negligible relative to the convection viscosity and bottom friction term. However the definition of the time-derivative used in this report differs from the RIPCEL definition.

Onset to a theoretical analysis

- Arthur (1962) has suggested that the narrowing of a rip current entering deeper water could be explained on basis of conservation of vorticity. It has been shown that dissipation of vorticity due to bottom friction is not very strong. This means that divergence of the streamlines cannot be explained on basis of dissipation of vorticity due to bottom friction.

- Large velocity gradients near the sidewall as observed in the laboratory can also be described by a model of cylindrical flow with a proper choice of the ratio of bottom friction coefficient and viscosity coefficient.

- An analysis of the time scales in the models learns that at least 70% of the final velocity should be present after one minute. Minor changes should be expected in the course of time.

- In offshore direction the observed rip current velocities tend to remain more or less constant while the calculated velocity distribution drops off rather fast.

- The observed discharge in the rip current in offshore direction is several times larger than the calculated discharge. This points towards a mechanism by which in the observed eddy mass from the eddy is entrained in the rip current. Such a mechanism seems not to act in the numerical model.

- The centre of rotation of the observed eddy is located much further offshore than is the case in the calculated eddy.

- The driving forces of the current pattern are much smaller than the forces creating set-up and set-down.

- The convective terms are mainly dominant in the outbreaking rip current.

- Bottom friction terms are important in the longshore current near the shoreline. In the large scale circulation just outside the breakerline the viscous (lateral mixing) terms dominate the bottom friction terms.

Recommendations

The interaction between longshore current, eddy and rip current is also to be expected in prototype. This may be the case in tidal areas near breakwaters and in a bar and gully system. The constant and high velocity in the offshore current can be important for coastal morphology. It is therefore regarded as very important that the mechanisms governing the concentrated offshore current become clear.
The degree of interaction between eddy, longshore current and offshore current will also influence the choice of the parameters for bottom friction and viscosity. Also from this point of view further detailed

analysis of laboratory experiments and numerical results is required. Together with the detailed analysis also effects such as wave-current interaction and 3-D effects should broadly be taken into account. In the calculated free water surface minor irregularities have been noticed. Their effect could be investigated by using a rigid lid model instead.

REFERENCES

1. ARTHUR, R.S. (1962)
   A note on the dynamics of rip currents
   J. of Geophysical Research; 67:7

2. BATTJES, J.A. (1974)
   Computation of set-up, longshore currents, run-up and overtopping due to wind generated waves
   Delft University of Technology

3. IWATA, N. (1970)
   A note on the wave set-up, longshore currents and undertows
   Journal of the Oceanographical Society of Japan
   Volume 26, No. 4, pp. 233-236

4. JAMES, I.D. (1972)
   Some nearshore effects of ocean waves
   Ph.D.Thesis, Cambridge University

5. LIU, P.L.F. and DALRYMPLE, R.A. (1978)
   Bottom frictional stresses and longshore currents due to waves with large angles of incidence
   Journal of Marine Research; 36:2:357-375

6. LONGUET-HIGGINS, M.S. (1970)
   Longshore currents generated by Obliquely Incident Sea Waves (1+2)
   Journal of Geophysical Research; 75:33:6778-6801

7. LONGUET-HIGGINS, M.S. (1972)
   Recent progress in the study of longshore currents in Waves on Beaches
   Academic Press, New York, pp. 203-248

8. STIVE, M.J.F. and WIND, H.G. (1982)
   A study of radiation stress and set-up in the nearshore region
   Coastal Engineering; 6:1:1-25

REFERENCES (Continued)

9. VISSER, P.J. (1982)
The proper longshore current in a wave basin
Communications on Hydraulics, Delft University of Technology, Report no. 82-1

10. VREUGDENHIL, C.B. (1980)
A method of computation for unsteady wave-driven coastal currents
Delft Hydraulics Laboratory; R 1174 part 1

11. VREUGDENHIL, C.B. (1978)
Keuze voor een rekenmethode voor twee-dimensionale kuststromingen
(in Dutch)
Delft Hydraulics Laboratory; R 1174 progress report 4

12. WIND, H.G. (1980)
Data of two experiments on wave driven coastal currents
Delft Hydraulics Laboratory; R 1174 progress report 6

13. WIND, H.G. (1982)
Testcases for RIPCEL
Delft Hydraulics Laboratory; R 1174 progress report 3

	wave basin of Delft Hydraulics Laboratory	wave basin of Delft University of Technology
waterdepth in the horizontal portion (m)	0.264	0.399
waveheight in the horizontal portion (m)	0.043	0.072
wave period (s)	1	2.01
angle between wave crest and slope	20^{o}	31.1^{o}
width of the breakerzone measured normal to the shore (m) from S.W.L. to breakerline	3.30	1.06
beach slope	1:50	1:10
breaker index	0.7	1.00

Table 1 Initial test conditions

SECTION IV			SECTION V		
distance from S.W.L. (m)	waveheight (m)	set-up (10^{-2} m)	distance from S.W.L. (m)	waveheight (m)	set-up (10^{-2} m)
- 0.25	0	0.50	- 0.25	0	0.50
0.91	0.007	-	1.09	0.007	-
1.41	0.010	-	1.59	0.010	0.31
1.91	0.017	0.24	2.09	0.019	0.16
2.41	0.027	0.09	2.59	0.028	0.03
2.91	0.038	-0.09	3.09	0.040	-0.03
3.41	0.052	-	3.59	0.049	-0.10
3.91	0.048	-	4.09	0.048	-0.10
4.41	0.050	-	4.59	0.049	-0.09

Table 2 Wave height and set-up in basin 1;(test B)

distance from S.W.L.(m)	velocity parallel to the side wall (m/s)			distance from S.W.L.	velocity parallel to the shore (m/s)	
	section I	section II	section III		section IV	section V
0.25	0.13	0.13	0.09	0.50	0.05	0.03
0.50	0.14	0.12	0.10	1.00	0.11	0.06
0.75	0.13	0.09	0.10	1.50	0.17	0.15
1.25	0.08	0.06	0.05	4.50	0.05	0.04
1.75	0.03	0.04	0.03	5.00	0.04	0.03
				5.50	0.03	0.03

Table 3 Velocity field in basin 1;(test B)

SECTION III		
distance from S.W.L. (m)	waveheight (m)	set-up (10^{-2} m)
0.11	0.029	1.76
0.31	0.048	0.76
0.51	0.058	0.02
0.71	0.075	-0.03
0.91	0.098	-0.02
1.11	0.103	-0.02
1.31	0.096	-0.01
1.51	0.083	-0.01
1.71	0.074	-0.01
1.90	0.075	-0.01
2.10	0.077	-0.01

Table 4 Wave height and set-up in basin 2

distance from S.W.L. (m)	mean water depth $(h+\bar{\eta})$ (m)	velocity parallel to the shore (m/s)				
		section I	section II	section III	section IV	section V
-0.29	-	0.257	0.371	0.382	0.336	0.348
0.09	0.018	0.569	0.538	0.559	0.495	0.421
0.11	0.028	0.665	0.649	0.627	0.553	0.447
0.31	0.038	0.670	0.645	0.623	0.493	0.387
0.51	0.050	0.612	0.591	0.584	0.428	0.236
0.71	0.067	0.556	0.408	0.420	0.260	0.088
0.91	0.088	0.345	0.222	0.196	0.134	0.077
1.11	0.108	0.160	0.107	0.139	0.118	0.068
1.31	0.129	0.058	0.094	0.117	0.123	0.071
1.51	0.149	0.039	0.091	0.107	0.123	0.071
1.70	0.169	0.035	0.088	0.106	0.121	0.068
1.90	0.189	0.035	0.087	0.097	0.119	0.068
2.10	0.209	0.033	0.084	0.087	0.114	0.070
2.30	0.229	0.035	0.082	0.087	0.115	0.067
2.70	0.270	0.036	0.080	0.084	0.111	0.069

Table 5 Longshore velocity distribution in basin 2

distance from the sidewall (m)	velocity parallel to the wall (m/s)	
	section VII	section VI
0.20	0.201	0.045
0.40	0.170	0.045
0.80	0.134	0.046
1.20	0.104	0.052
1.60	0.085	0.046
2.00	0.070	0.047

Table 6 Velocity distribution parallel to the sidewalls in basin 2

K	J	time derivative	convection	viscosity	bottom friction	pressure gradient	wave pressure gradient
2	4	-1.64	0.98	0.28	0.18	-2.52	2.71
8	4	0.22	0.19	0.16	0.77	-4.09	2.74
14	4	0.69	0.05	-0.03	0.73	-4.17	2.73
20	4	-0.92	-0.41	-0.24	0.03	-1.17	2.72
2	8	1.23	0.01	0.60	0.07	-0.39	-1.52
8	8	-0.31	0.06	-0.85	0.24	2.40	-1.53
14	8	1.12	-0.26	-0.95	0.33	1.30	-1.53
20	8	1.10	-0.81	-0.07	0.19	0.97	-1.53
2	12	-1.10	0.04	0.08	0.00	1.69	-0.71
8	12	-1.22	0.02	-0.11	-0.04	2.07	-0.72
14	12	0.82	-0.02	-0.39	-0.05	0.35	-0.72
20	12	0.59	-0.29	0.17	0.00	0.24	-0.72
2	16	0.48	0.00	0.07	0.00	-0.16	-0.38
8	16	-0.61	0.00	0.10	-0.02	0.92	-0.38
14	16	-0.28	0.02	-0.04	-0.03	0.72	-0.39
20	16	-0.09	0.00	0.07	0.00	-0.41	-0.39

Table 7 Magnitude of the terms in the (longshore) p-equation after t = 56 s (10^{-4} m^2/s^2)

K	J	time derivative	convection	viscosity	bottom friction	pressure head	wave pressure gradient
2	4	-0.34	-0.22	0.21	-0.22	-11.64	12.21
8	4	-1.08	-0.07	0.12	-0.49	-10.85	12.37
14	4	0.28	0.15	0.17	-0.37	-12.52	12.30
20	4	-0.42	0.08	-0.31	0.06	-11.61	12.21
2	8	-0.52	-0.10	-0.30	-0.32	5.55	- 4.30
8	8	0.71	0.02	-0.68	-0.20	4.48	- 4.32
14	8	1.47	0.21	-0.86	-0.14	3.64	- 4.32
20	8	4.68	0.63	-0.23	0.68	- 1.45	- 4.31
2	12	1.09	-0.06	-0.20	-0.09	1.27	- 2.00
8	12	-0.03	-0.01	0.00	0.00	2.08	- 2.04
14	12	-0.40	-0.00	-0.23	0.06	2.61	- 2.03
20	12	-0.69	-0.48	0.55	0.40	2.25	- 2.03
2	16	-0.65	0.00	-0.04	-0.02	0.50	- 1.09
8	16	-0.20	-0.00	0.00	0.01	1.30	- 1.11
14	16	-0.81	-0.03	0.08	0.04	1.83	- 1.11
20	16	-1.35	-0.22	0.48	0.15	2.06	- 1.12

Table 8 Magnitude of the terms in the q-equation after t = 56 s (10^{-4} m^2/s^2)

J \ K	2	4	6	8	10	12	14	16	18	20	22
18	97	- 49	373	117	149	263	- 20	25	-159	23	
16	- 13	- 23	183	159	203	- 93	73	-106	- 33	- 49	
14	62	- 11	42	199	155	27	- 44	-148	- 95	- 83	
12	16	- 50	- 18	170	99	20	-115	-152	-148	-174	
10	12	- 40	- 20	93	18	- 10	-120	-165	- 87	- 72	
8	- 81	- 38	70	20	- 3	- 9	- 73	-114	34	2	
6	22	20	- 10	- 2	- 2	0	19	37	34	2	
4	- 60	23	- 75	8	2	11	25	38	9	- 33	
2	45	26	- 10	8	5	22	16	0	- 5	3	

Table 9 p-equation; 100x time derivative/gradient in wave action

J \ K	2	4	6	8	10	12	14	16	18	20	22
18	- 1	1	- 1	0	0	- 1	- 3	- 3	0	- 3	
16	0	1	0	- 1	- 2	- 2	- 4	- 2	0	- 1	
14	0	0	0	- 2	- 2	- 3	- 2	- 2	0	13	
12	- 6	0	0	- 3	- 2	0	3	6	16	40	
10	- 6	- 5	- 6	- 4	0	2	9	25	56	67	
8	0	- 13	- 17	- 4	- 2	6	17	41	91	53	
6	18	9	5	5	15	- 3	0	-15	-48	-35	
4	36	7	- 5	7	12	3	2	- 8	-21	-15	
2	9	10	- 4	18	15	5	6	5	0	0	

Table 10 p-equation; 100x convection/gradient in wave action

J \ K	2	4	6	8	10	12	14	16	18	20	22
18	39	-15	-37	-52	-33	-21	6	-14	-15	19	
16	-17	-18	-37	-26	-14	7	10	- 8	-22	-18	
14	8	-19	-28	- 5	4	24	24	15	- 1	10	
12	-11	-14	- 5	15	22	44	54	44	28	-23	
10	-35	- 7	25	38	45	65	76	63	46	3	
8	-40	41	50	55	58	63	63	42	15	- 5	
6	14	42	41	41	43	42	42	45	43	- 6	
4	11	11	7	6	5	1	- 1	- 4	- 1	- 9	
2	- 1	- 4	- 7	- 7	- 8	-10	-12	-13	- 8	- 2	

Table 11 p-equation; 100x viscosity terms/gradient in wave action

J \ K	2	4	6	8	10	12	14	16	18	20	22
18	4	6	6	6	6	7	7	6	5	3	
16	2	4	5	6	6	7	7	7	5	3	
14	3	4	6	6	7	7	8	8	7	3	
12	0	3	5	6	6	7	7	7	5	0	
10	- 3	0	0	0	0	0	0	- 2	- 4	- 6	
8	- 4	-13	-14	-16	-19	-20	-21	-24	-23	-13	
6	2	21	23	24	26	27	27	27	22	6	
4	7	26	27	28	29	28	27	23	15	1	
2	13	22	22	22	22	19	15	7	1	- 2	

Table 12 p-equation; 100x bottom friction/gradient in wave action

J \ K	2	4	6	8	10	12	14	16	18	20	22
18	-239	395	-442	-170	-222	179	- 89	-114	-311	-446	
16	41	140	-251	-238	-294	-188	-186	10	- 67	-107	
14	-173	20	-120	-299	-263	-155	- 86	26	- 71	- 76	
12	-239	- 38	- 81	-288	-225	-171	- 49	- 5	- 54	- 34	
10	- 67	- 61	- 99	-227	-162	-157	- 65	- 22	- 50	9	
8	25	- 76	-125	-156	-135	-139	- 85	- 45	- 95	- 64	
6	-155	-192	-158	-169	-167	-166	-188	-193	-152	- 66	
4	- 93	-167	-122	-149	-148	-144	-153	-148	-102	- 43	
2	-165	-153	-100	-142	-134	-136	-125	-100	- 89	- 99	

Table 13 p-equation; 100x pressure head/gradient in wave action

J \ K	2	4	6	8	10	12	14	16	18	20	22
18	-117	75	-55	37	140	169	178	107	122	113	
16	- 60	63	-26	18	75	74	73	113	153	121	
14	- 63	26	11	- 9	28	- 2	40	76	73	97	
12	- 54	8	40	1	- 21	- 8	20	23	4	34	
10	- 21	9	36	- 6	- 15	- 4	- 11	- 23	- 32	- 66	
8	12	4	5	-16	- 2	- 28	- 34	- 31	- 51	-109	
6	- 9	- 4	- 2	- 5	- 2	2	3	5	12	19	
4	- 3	- 8	- 7	- 9	- 6	0	2	3	0	- 3	
2	- 9	- 5	- 3	- 6	7	13	10	- 4	- 7	- 13	

Table 14 q-equation; 100x time derivative/gradient in wave action

J \ K	2	4	6	8	10	12	14	16	18	20	22
18	0	0	0	0	0	0	2	3	5	10	
16	0	0	0	0	0	1	3	3	7	20	
14	2	0	0	0	0	1	2	4	10	27	
12	3	0	0	0	0	0	0	2	8	24	
10	4	0	1	0	0	0	- 1	- 3	- 5	4	
8	2	0	2	0	0	- 2	- 5	-12	-24	-15	
6	0	0	0	0	0	1	2	4	6	4	
4	- 2	0	0	0	0	0	1	2	1	0	
2	0	0	0	- 2	- 1	0	0	0	0	0	

Table 15 q-equation; 100x convection terms/gradient in wave action

J \ K	2	4	6	8	10	12	14	16	18	20	22
18	0	- 7	- 8	- 3	- 7	- 1	-14	-15	-18	-38	
16	3	- 5	0	0	- 6	- 1	- 7	- 2	-11	-43	
14	2	- 4	3	0	- 6	- 1	5	5	- 6	-44	
12	10	0	2	0	- 1	9	11	12	4	-27	
10	12	4	2	5	12	13	16	18	13	-13	
8	7	11	10	16	20	20	20	21	19	5	
6	2	- 3	- 4	- 5	- 5	- 5	- 4	- 5	- 5	- 7	
4	2	2	0	0	0	0	1	0	- 1	- 3	
2	2	2	0	0	1	- 1	0	0	0	0	

Table 16 q-equation; 100x viscosity terms/gradient in wave action

J \ K	2	4	6	8	10	12	14	16	18	20	22
18	0	- 1	- 2	- 2	- 3	- 3	- 4	- 5	- 7	- 9	
16	2	0	0	- 1	- 2	- 3	- 4	- 5	- 8	-13	
14	3	0	0	0	- 2	- 3	- 4	- 6	- 9	-17	
12	4	1	0	0	- 1	- 2	- 3	- 5	-10	-20	
10	6	2	1	1	0	0	- 1	- 3	- 9	-20	
8	7	5	5	5	5	5	3	0	- 5	-16	
6	- 2	- 3	- 3	- 3	- 3	- 3	- 3	- 2	0	2	
4	- 2	- 3	- 4	- 4	- 4	- 4	- 3	- 2	0	0	
2	- 2	- 2	- 4	- 3	- 3	- 2	- 1	0	0	0	

Table 17 q-equation; 100x bottom friction/gradient in wave action

J \ K	2	4	6	8	10	12	14	16	18	20	22
18	15	-168	- 37	-133	-231	-254	-260	-190	-202	-176	
16	- 47	-158	- 73	-117	-167	-161	-165	-209	-241	-184	
14	- 44	-123	-114	- 91	-121	- 95	-143	-179	-167	-164	
12	- 63	-110	-142	-102	- 77	-115	-128	-133	-107	-111	
10	-102	-117	-140	-100	- 97	-109	-102	- 88	- 66	- 4	
8	-129	-126	-122	-104	-123	- 95	- 84	- 79	- 38	34	
6	- 91	- 90	- 90	- 87	- 91	- 95	- 97	-103	-113	-118	
4	- 95	- 90	- 89	- 88	- 90	- 97	-102	-103	- 99	- 95	
2	- 91	- 94	- 94	- 90	-104	-112	-110	- 95	- 91	- 87	

Table 18 q-equation; 100x pressure head/gradient in wave action

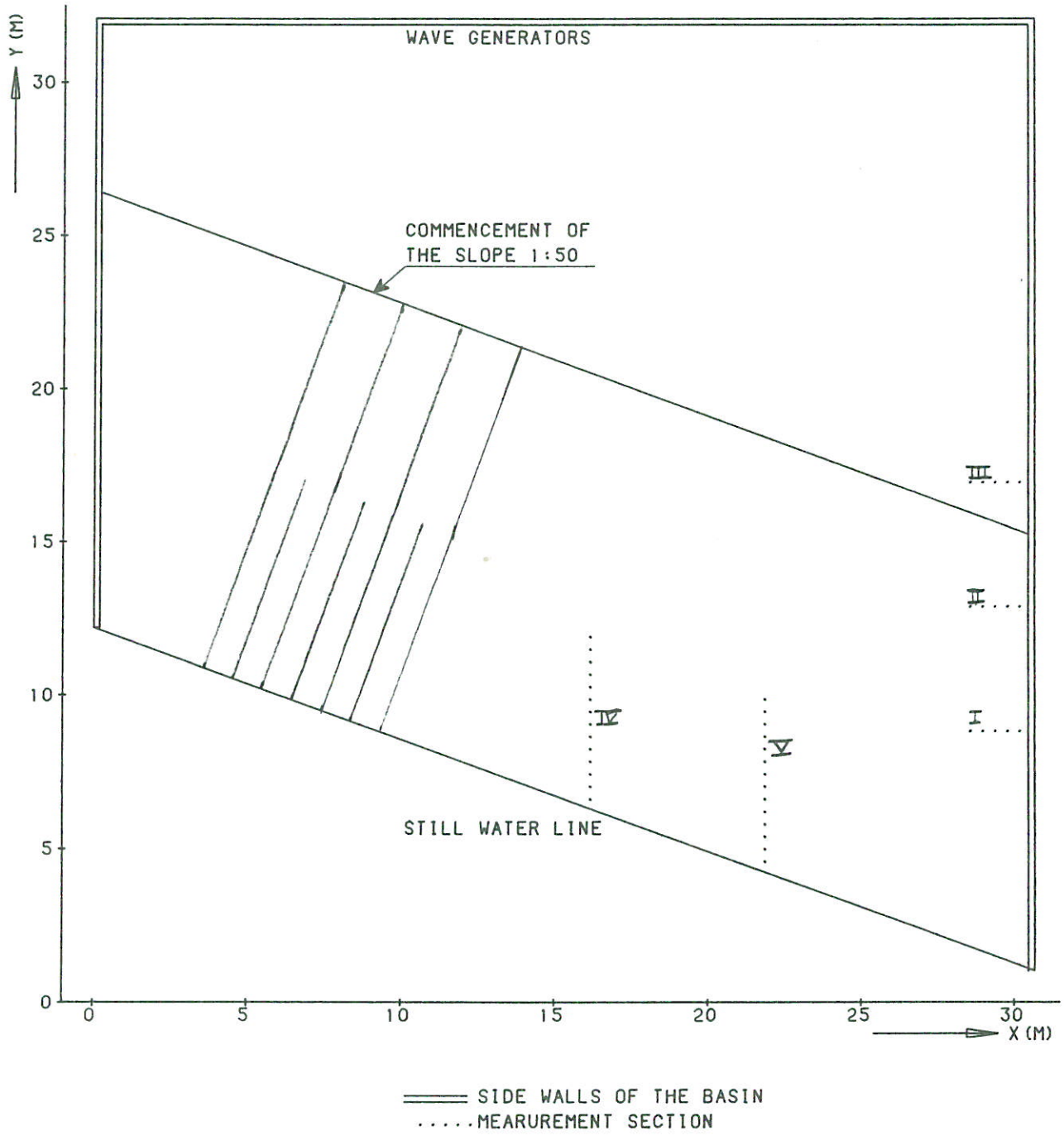

LAYOUT OF BASIN 1
(DELFT HYDRAULICS LABORATORY)

DELFT HYDRAULICS LABORATORY	R 1174	FIG. 1

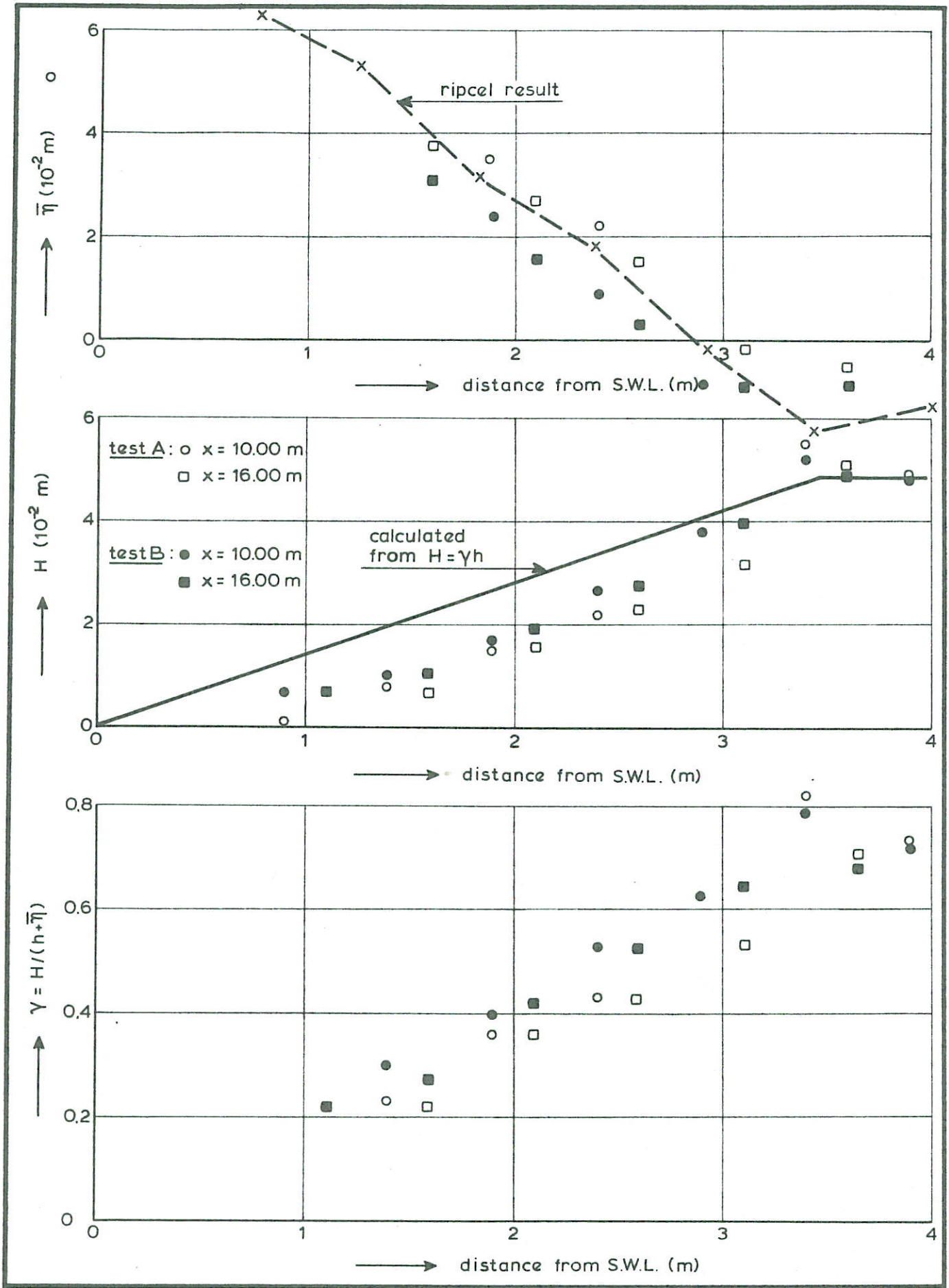

WAVE CONDITIONS AND SET-UP IN BASIN 1

DELFT HYDRAULICS LABORATORY | R 1174 | FIG. 2

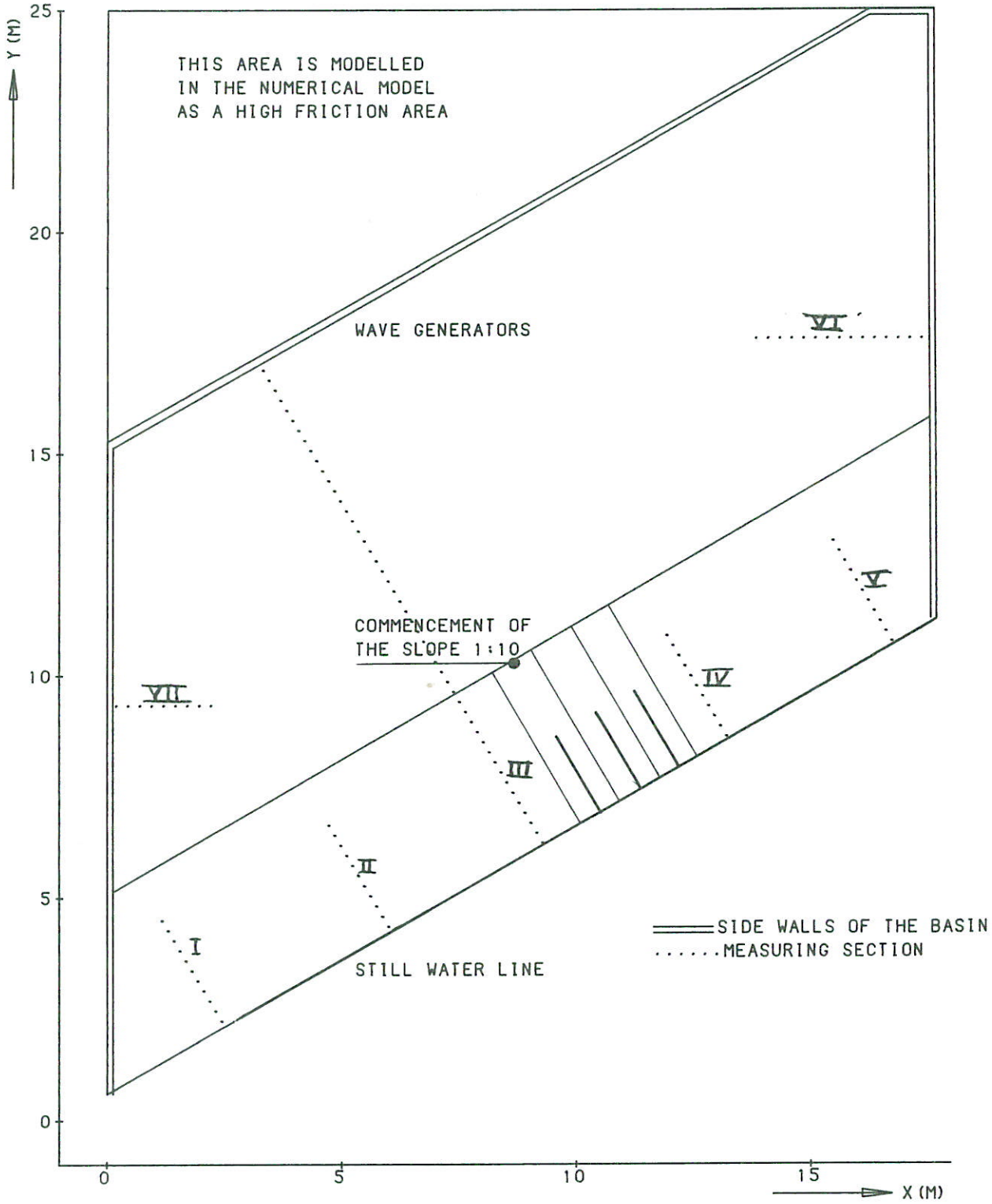

LAYOUT OF BASIN 2
(DELFT UNIVERSITY)

DELFT HYDRAULICS LABORATORY | R 1174 | FIG. 3

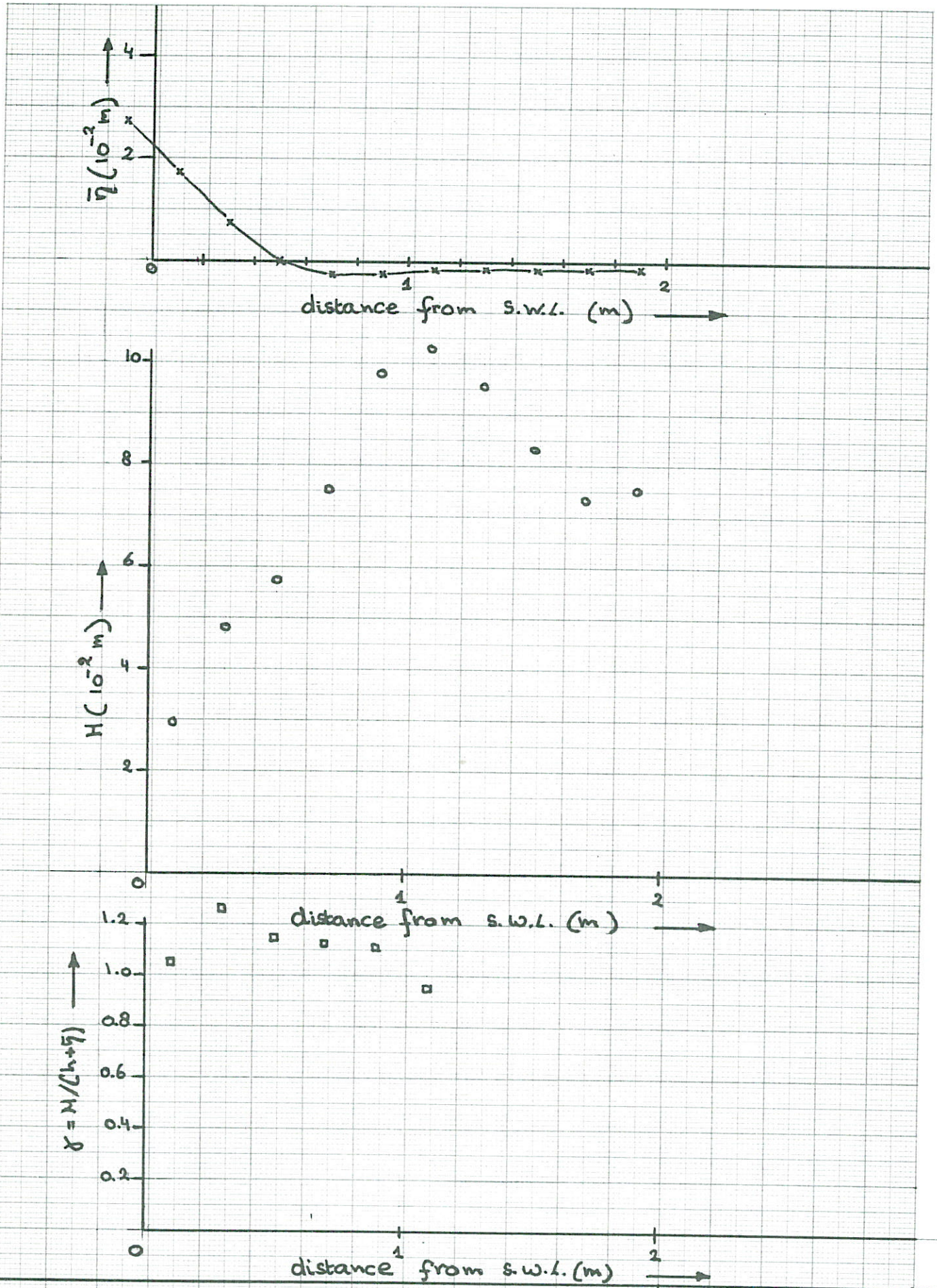

WAVE CONDITIONS AND SET-UP IN BASIN 2

DELFT HYDRAULICS LABORATORY

R1174 | FIG 4

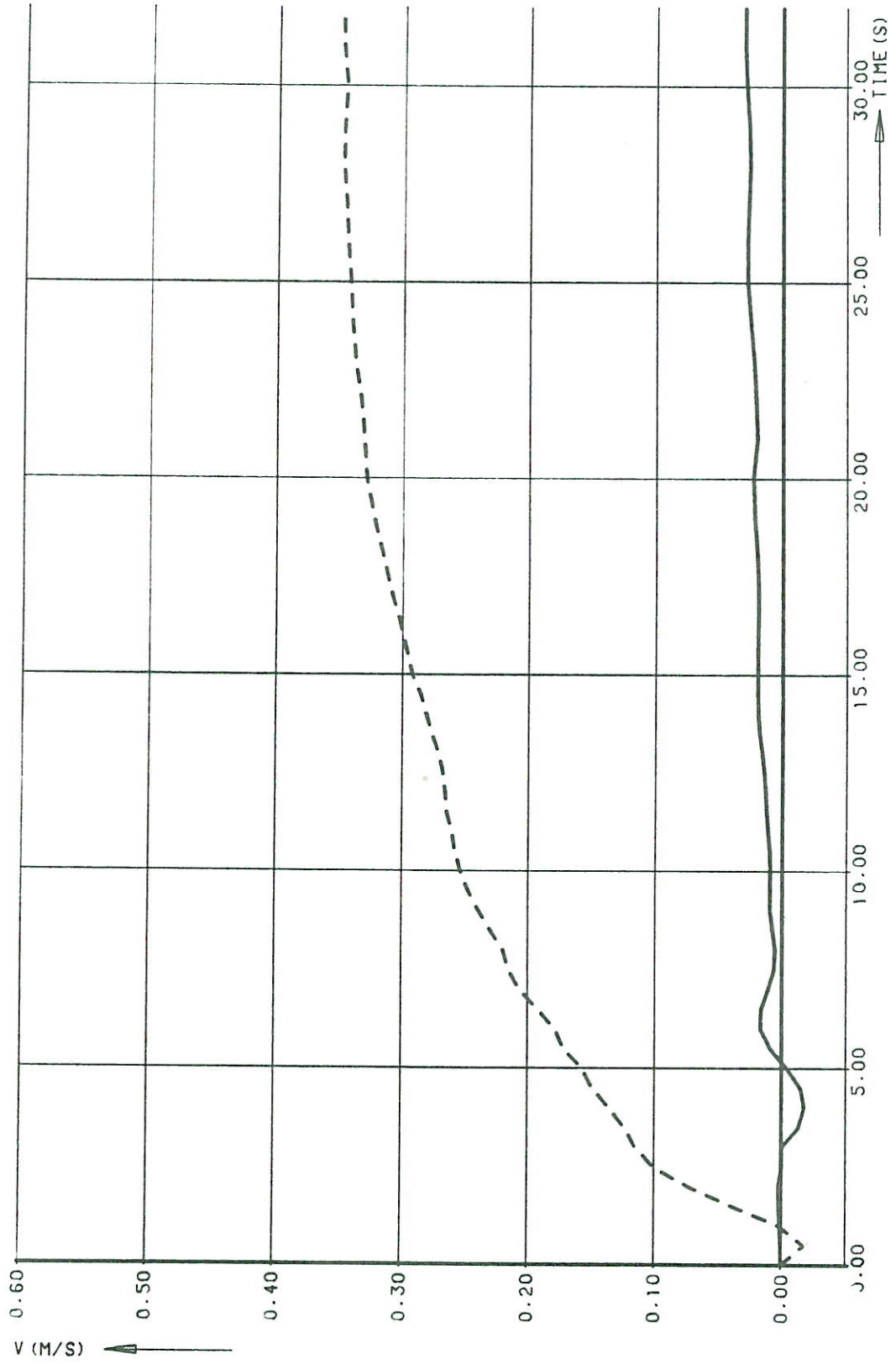

EVOLUTION OF THE VELOCITY

DELFT HYDRAULICS LABORATORY | R1174 | FIG. 5

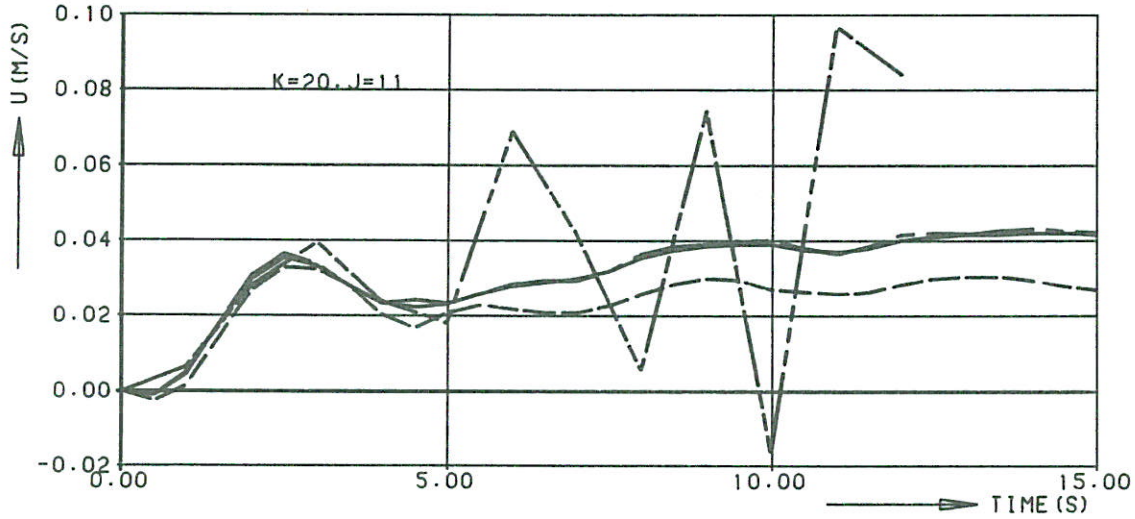

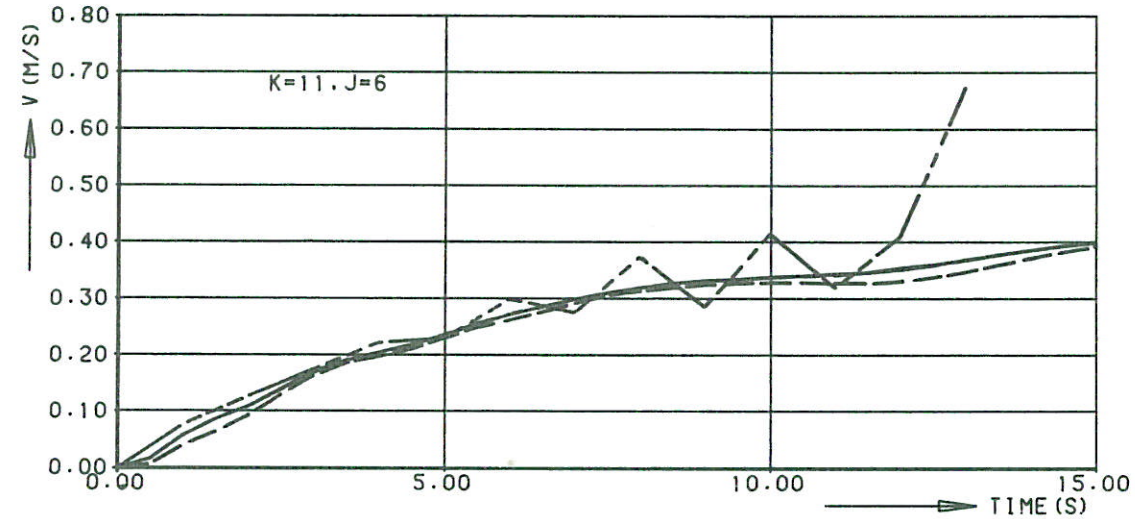

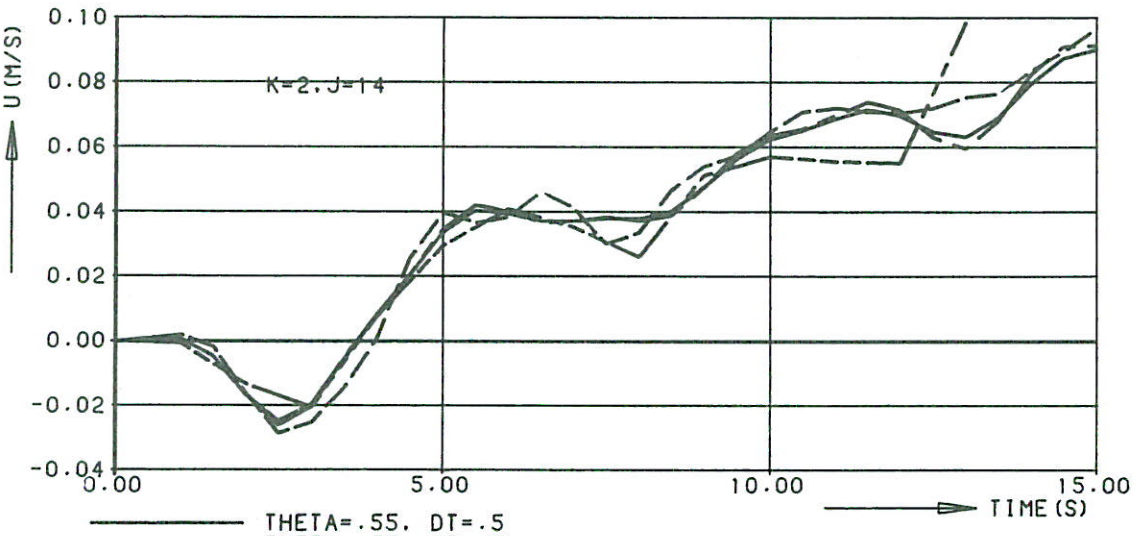

THETA=.55, DT=.5
THETA=.53, DT=.5
THETA=.53, DT=1
THETA=.53 DT=.1
for K,J see figure 8

EFFECT OF VARIATION OF Θ (THETA) AND TIMESTEP DT

DELFT HYDRAULICS LABORATORY | R1174 | FIG. 6

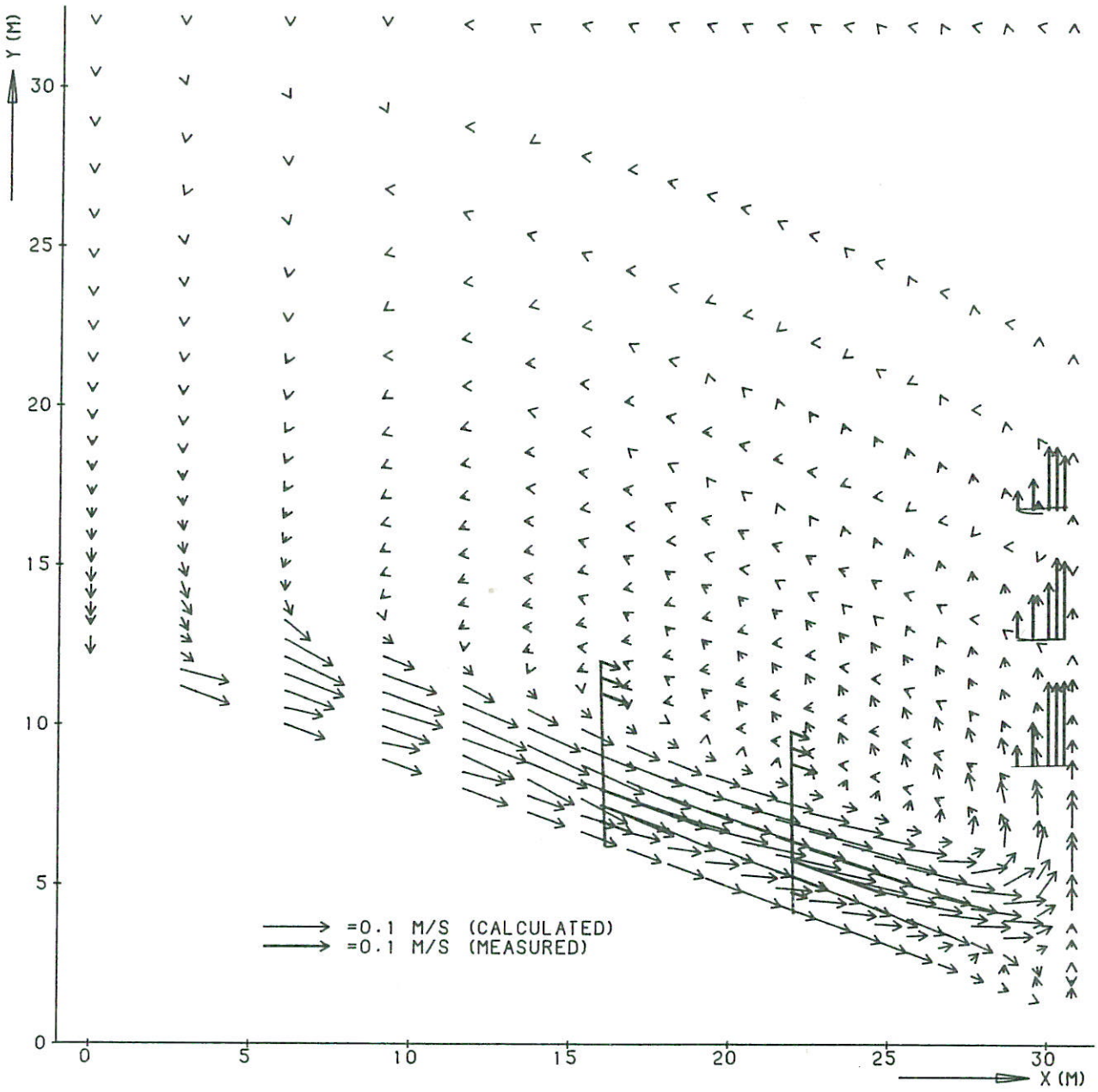

CURRENT PATTERN IN BASIN 1
(INCLUDING ALL TERMS) T=32 S.

DELFT HYDRAULICS LABORATORY | R 1174 | FIG. 7

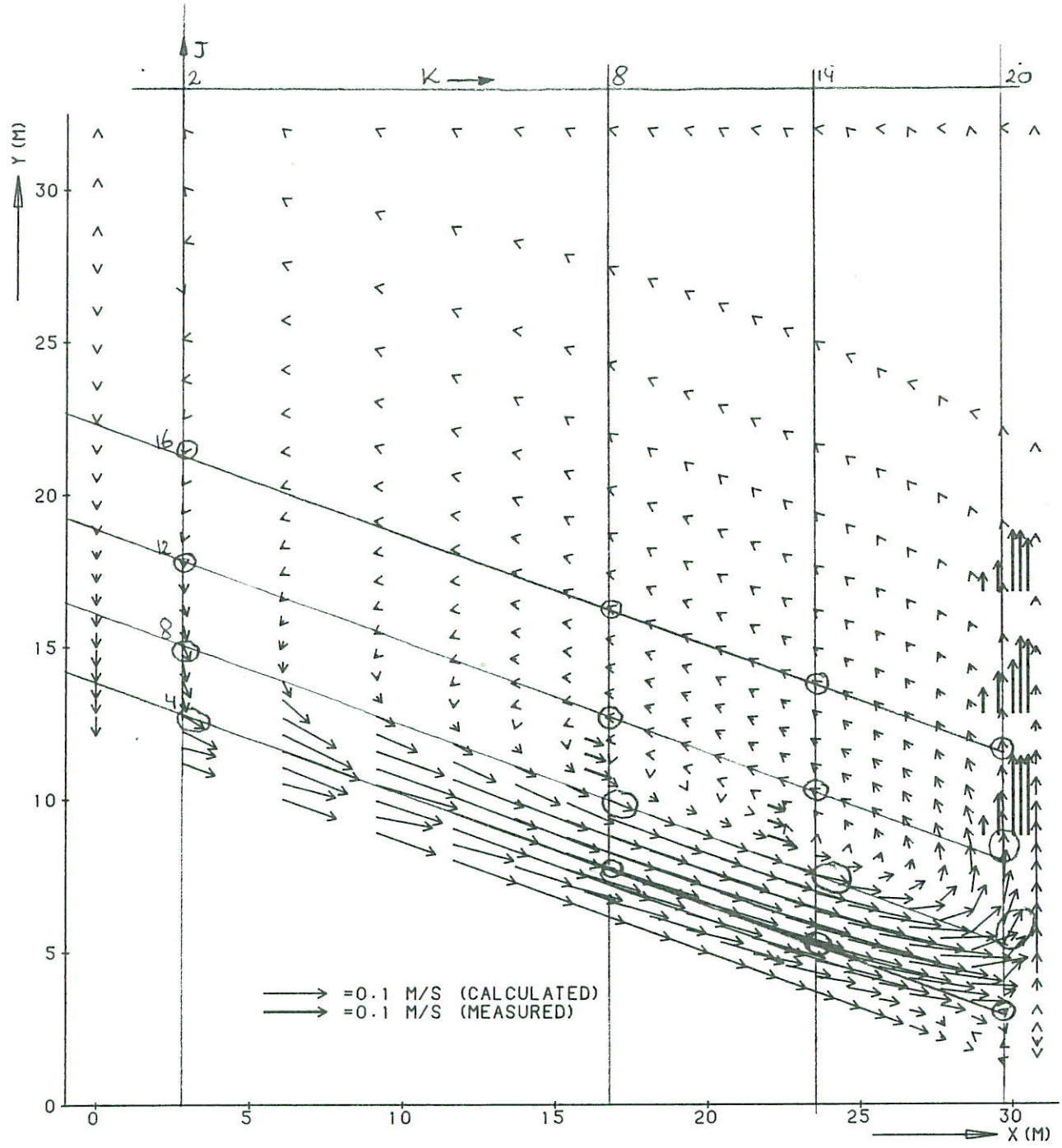

CURRENT PATTERN IN BASIN 1
(INCLUDING ALL TERMS) T=56 S.

DELFT HYDRAULICS LABORATORY | R 1174 | FIG. 8

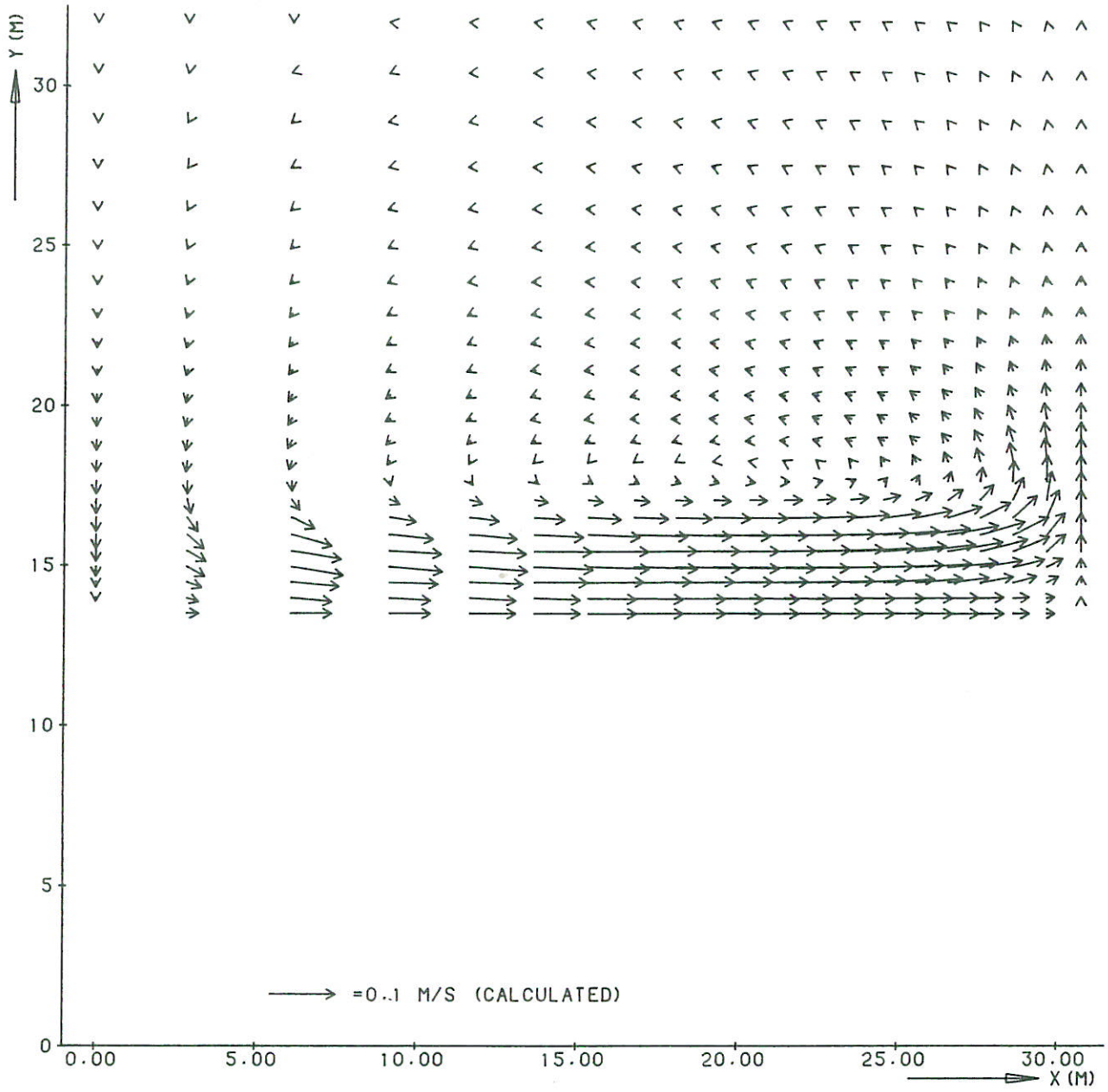

CURRENT PATTERN IN A RECTANGULAR BASIN
(INCLUDING ALL TERMS) T=32 S.

DELFT HYDRAULICS LABORATORY | R 1174 | FIG. 9

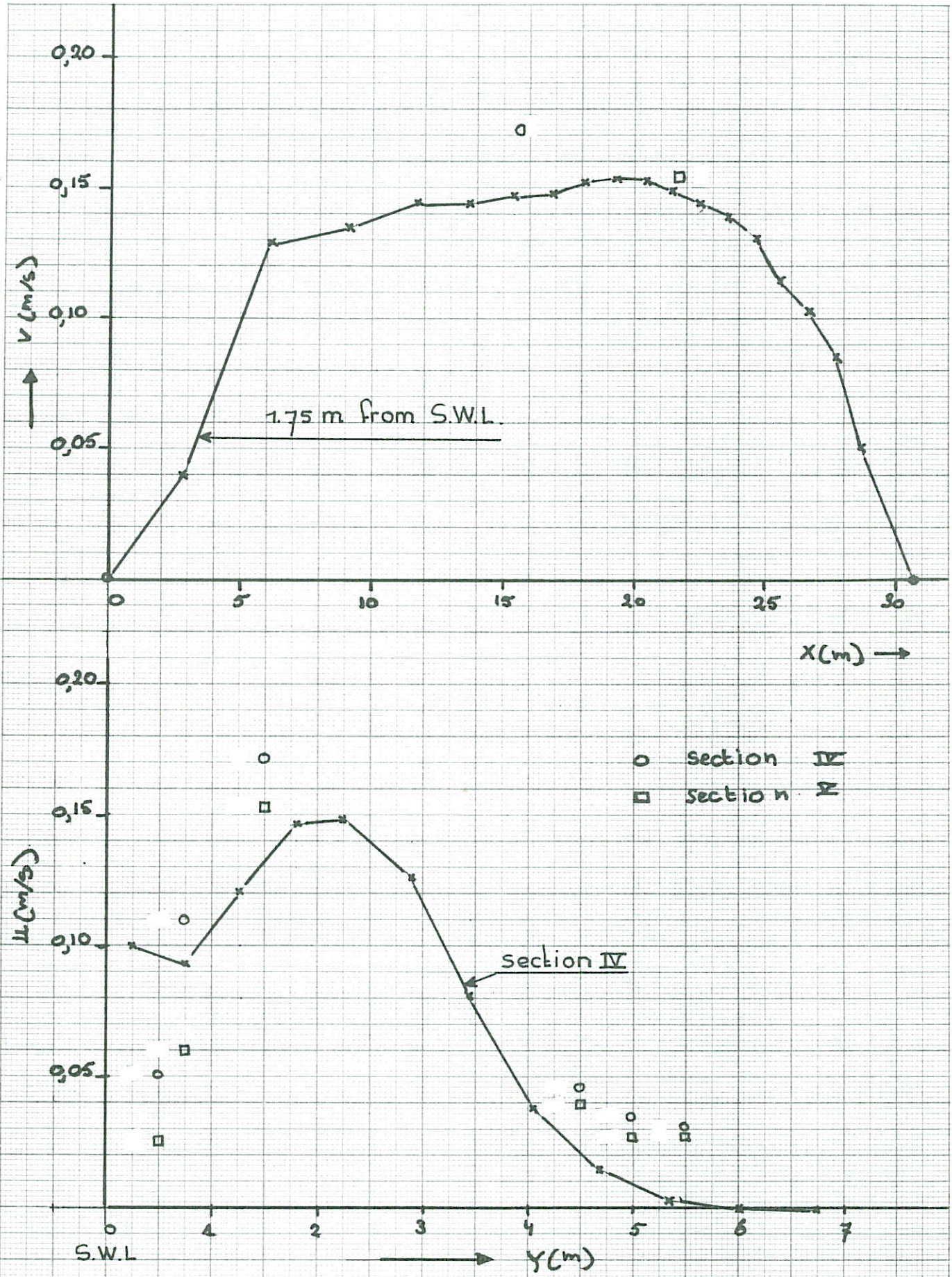

LONGSHORE CURRENT DISTRIBUTION IN BASIN 1

DELFT HYDRAULICS LABORATORY | R1174 | FIG 10

INTEGRATED DISCHARGE IN SECTION III OF BASIN 2

DELFT HYDRAULICS LABORATORY | R 1174 | FIG 11

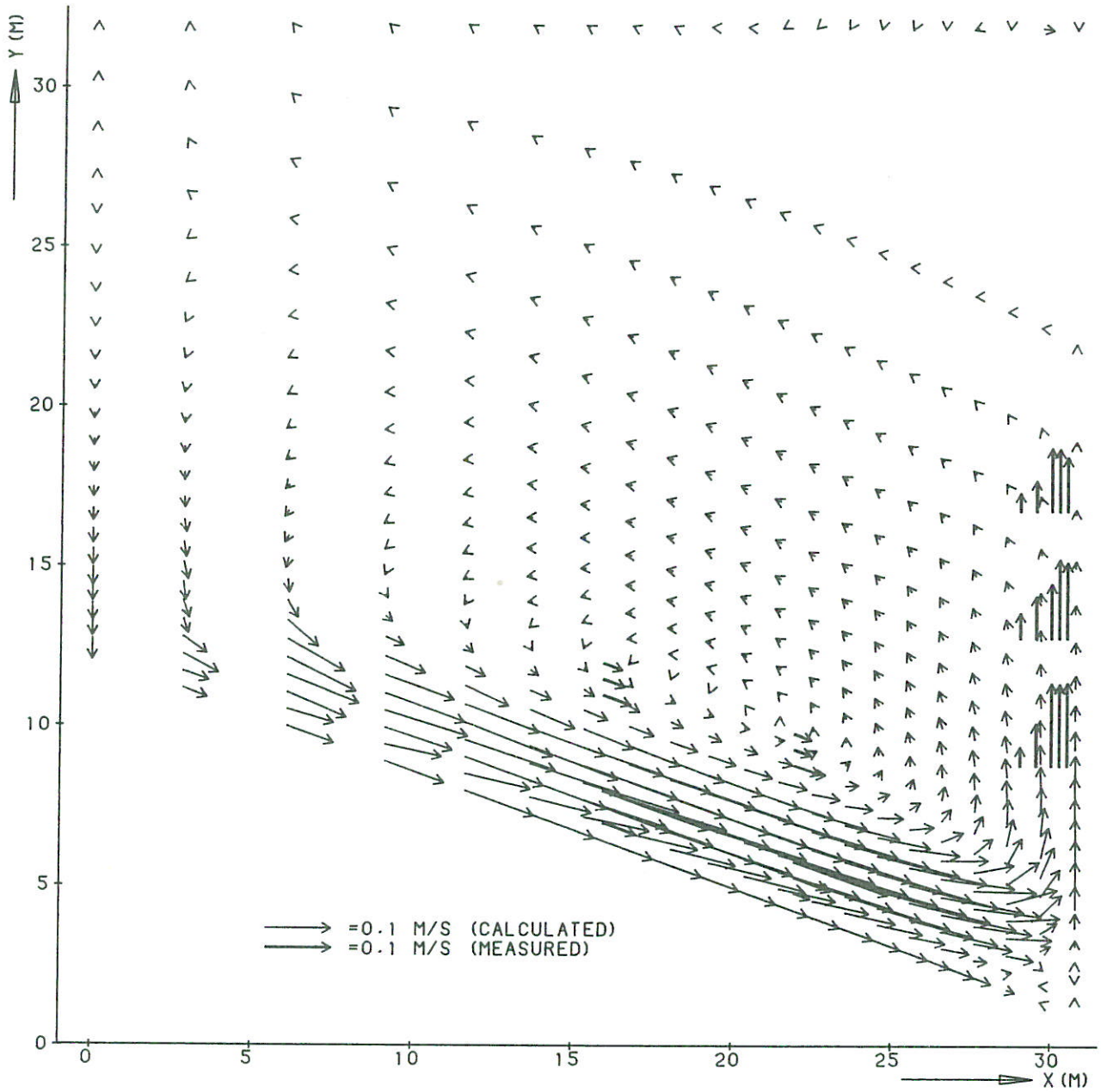

CURRENT PATTERN IN BASIN 1
(EXCLUDING CONVECTIVE TERMS) T=56 S.

DELFT HYDRAULICS LABORATORY | R 1174 | FIG. 12

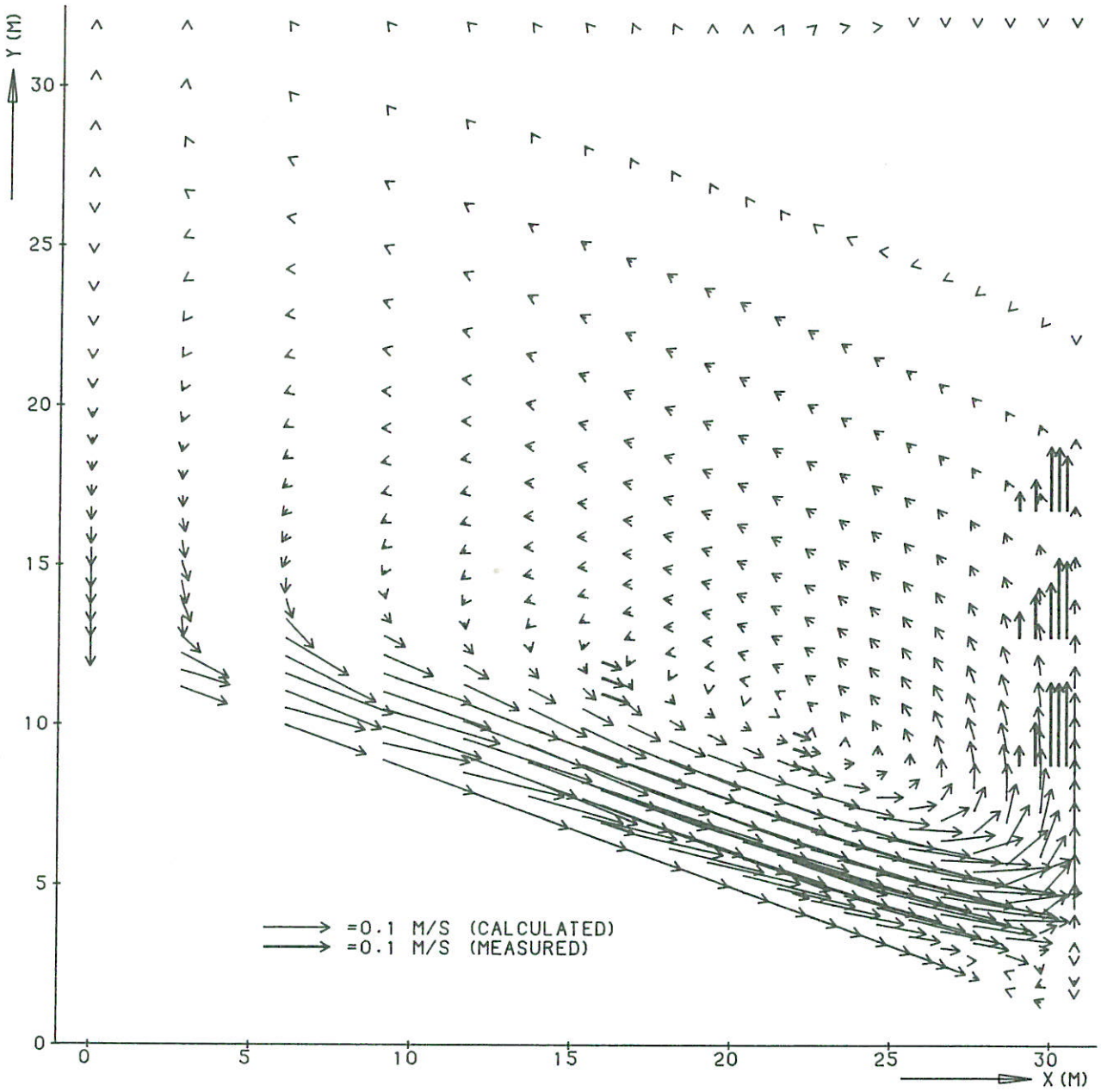

CURRENT PATTERN IN BASIN 1
(EXCLUDING BOTTOMFRICTION TERMS) T=56 S.

DELFT HYDRAULICS LABORATORY | R 1174 | FIG. 13

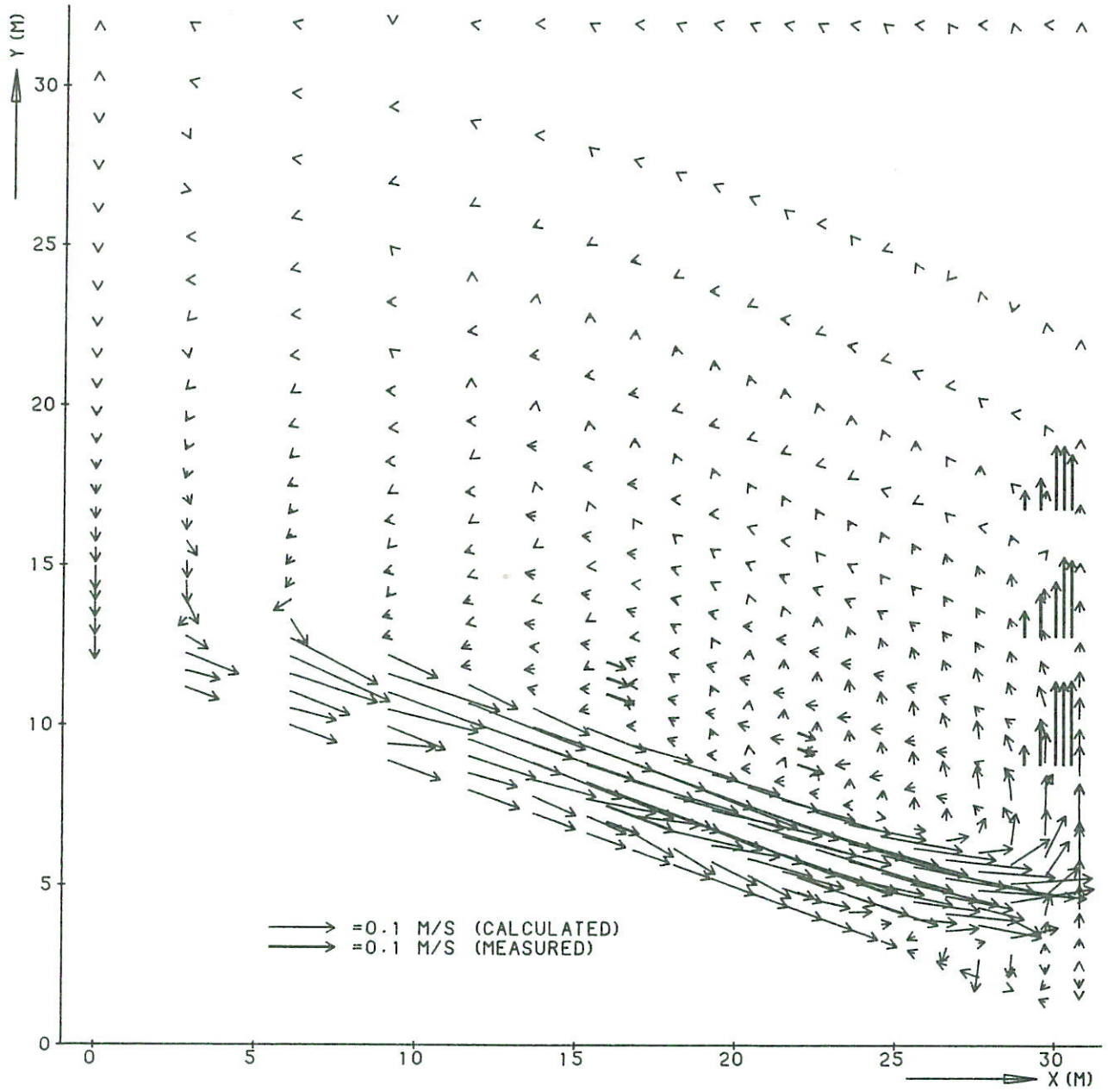

CURRENT PATTERN IN BASIN 1
(EXCLUDING VISCOUS TERMS) T=56 S.

DELFT HYDRAULICS LABORATORY | R 1174 | FIG. 14

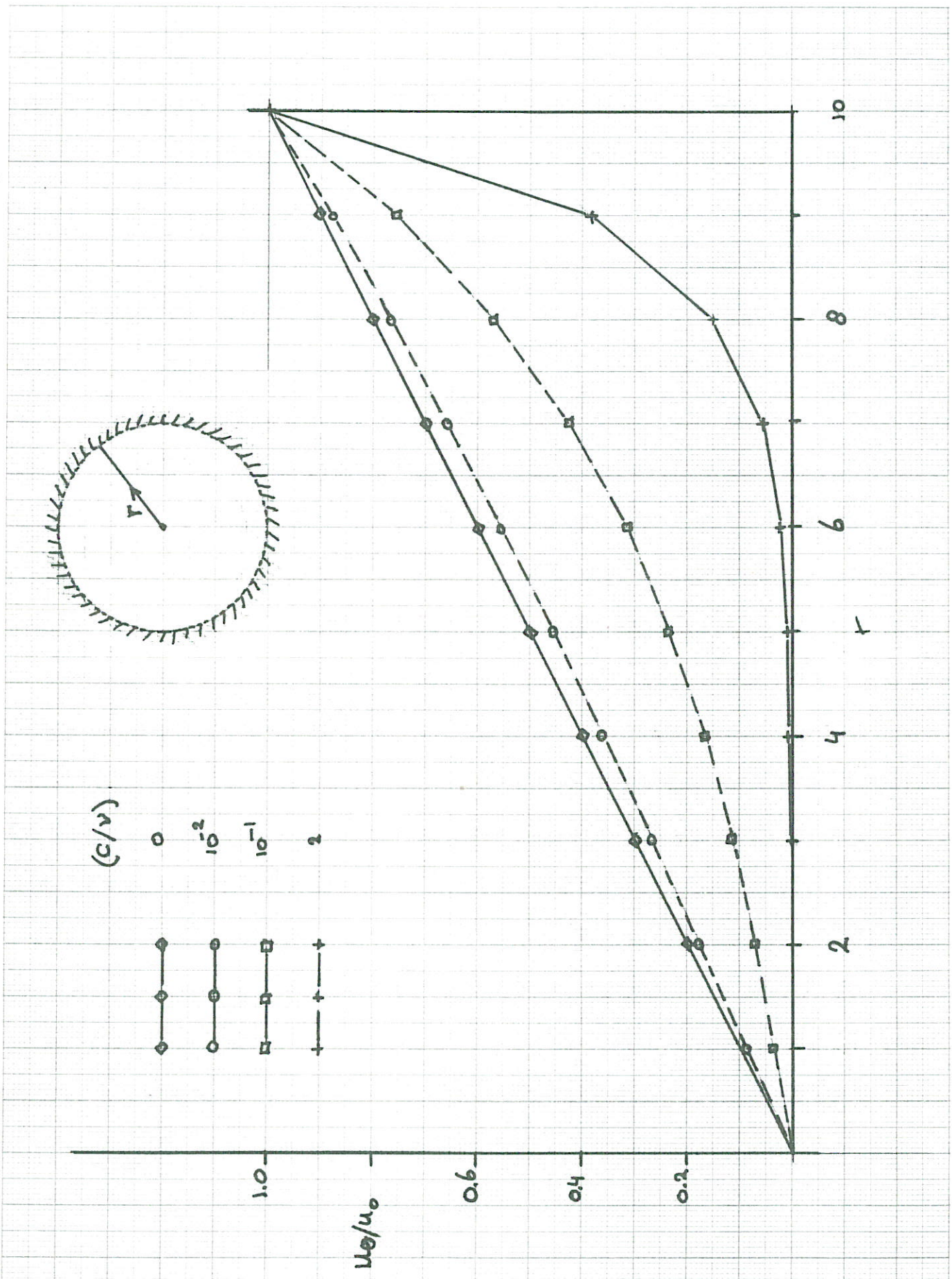

VELOCITY FIELD IN A CIRCULAR BASIN

GOVERNED BY BOTTOM FRICTION AND LATERAL MIXING

DELFT HYDRAULICS LABORATORY | R1174 | FIG 15.

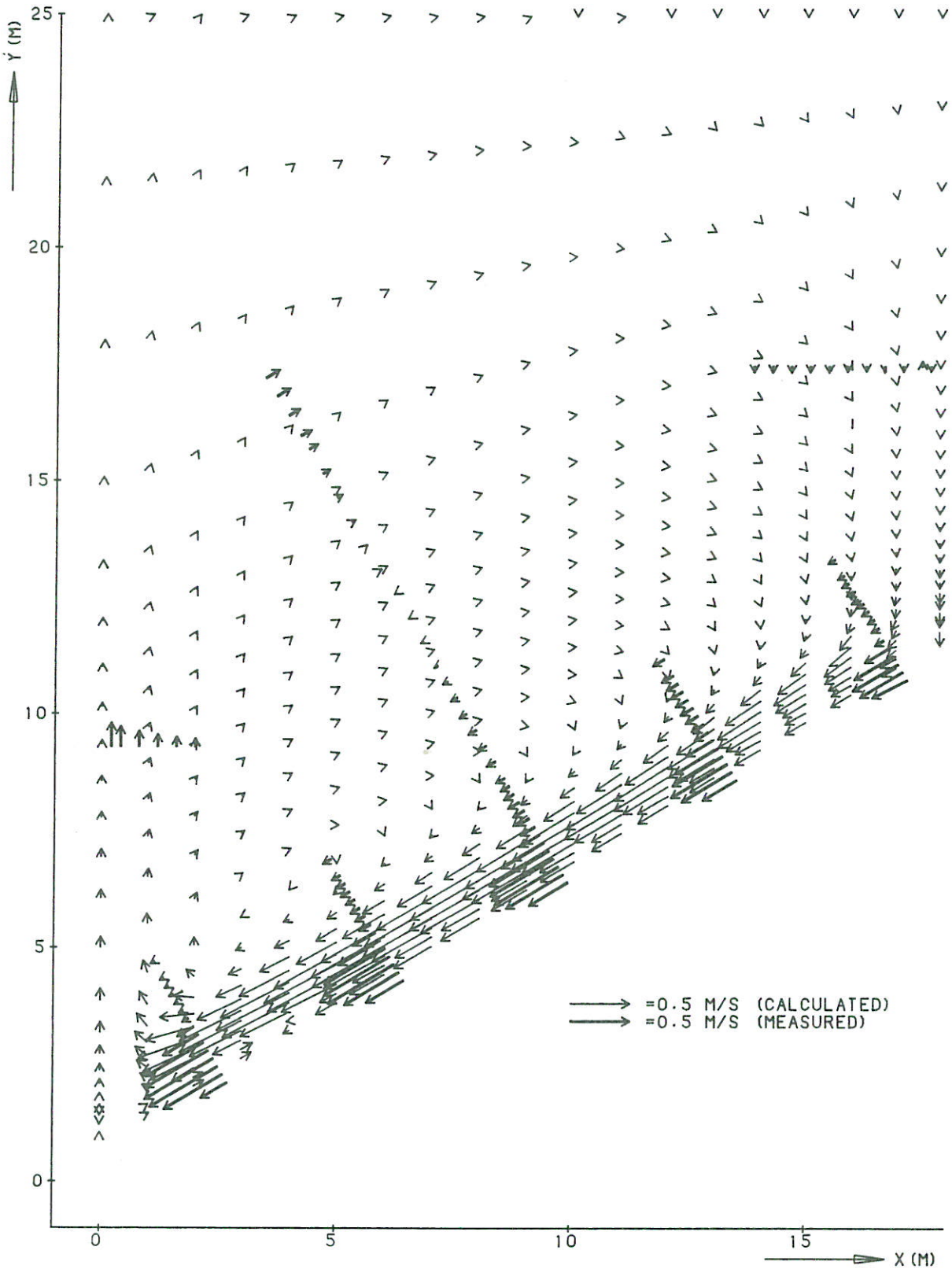

CURRENT PATTERN IN BASIN 2
(INCLUDING ALL TERMS) T=32 S.

DELFT HYDRAULICS LABORATORY | R 1174 | FIG. 16

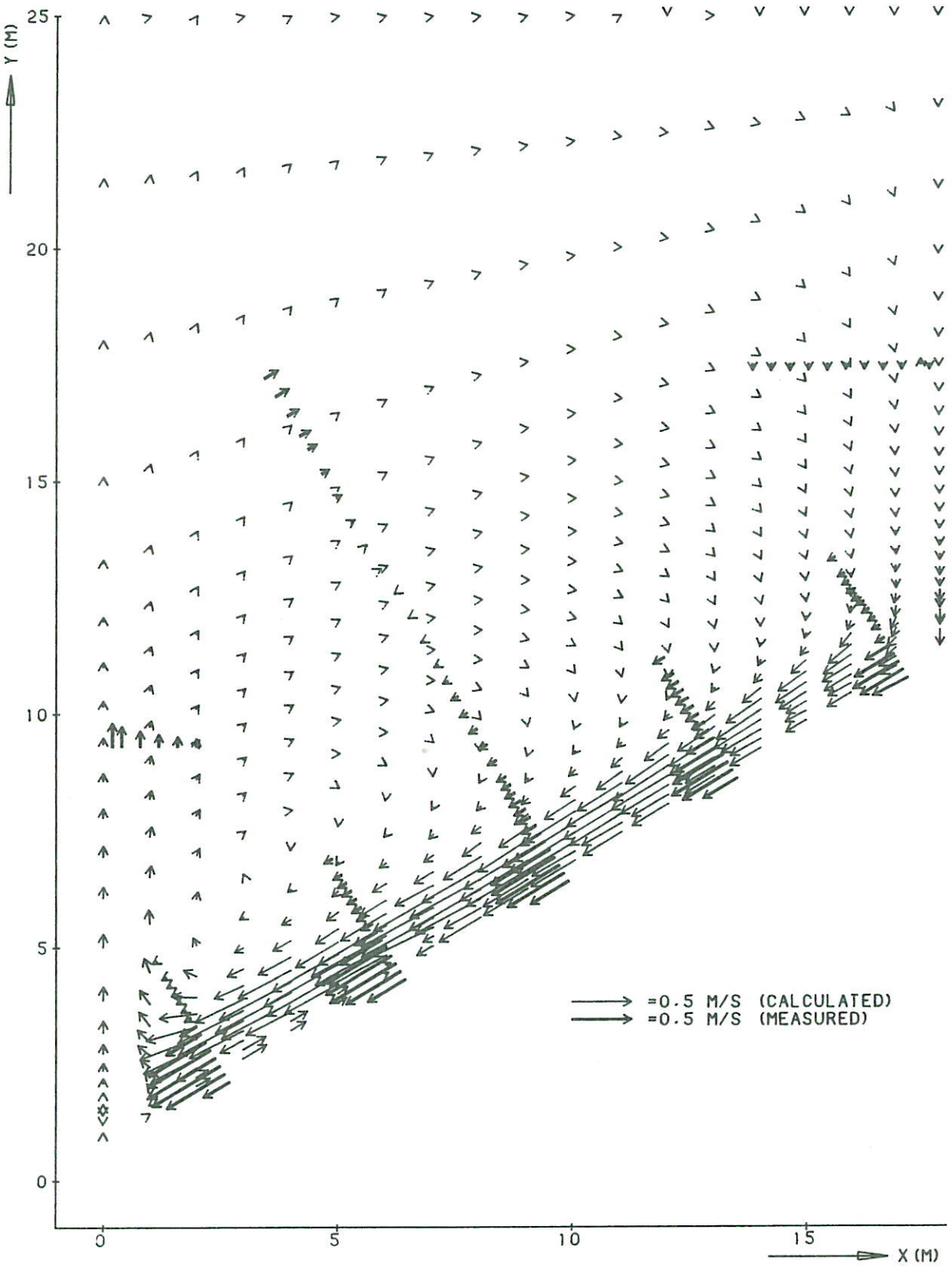

CURRENT PATTERN IN BASIN 2
(INCLUDING ALLTERMS) T=56 S.

DELFT HYDRAULICS LABORATORY | R 1174 | FIG. 17

APPENDIX A CONTINUITY EQUATION AND EQUATIONS OF MOTION

The equations of the mathematical model for unsteady wave driven coastal currents averaged over depth and wave period are presented and discussed in [12]. Here only a summary will be given. The continuity equation and the two momentum equations are:

$$\frac{\partial h}{\partial t} + \frac{\partial p}{\partial x} + \frac{\partial q}{\partial y} = 0 \qquad (A.1)$$

$$\frac{\partial p}{\partial t} + \frac{\partial}{\partial x}(p^2/h) + \frac{\partial}{\partial y}(pq/h) + gh\left(\frac{\partial h}{\partial x} + \frac{\partial z_b}{\partial x}\right) +$$

$$- \tau_{sx}/\rho + \tau_{bx}/\rho + \frac{1}{\rho}\left(\frac{\partial S_{xx}}{\partial x} + \frac{\partial S_{xy}}{\partial y}\right) - \frac{1}{\rho}\left(\frac{\partial h\tau_{xx}}{\partial x} + \frac{\partial h\tau_{xy}}{\partial y}\right) = 0 \qquad (A.2)$$

$$\frac{\partial q}{\partial t} + \frac{\partial}{\partial x}(pq/h) + \frac{\partial}{\partial y}(q^2/h) + gh\left(\frac{\partial h}{\partial y} + \frac{\partial z_b}{\partial y}\right) - \tau_{sy}/\rho +$$

$$+ \tau_{by}/\rho + \frac{1}{\rho}\left(\frac{\partial S_{xy}}{\partial x} + \frac{\partial S_{yy}}{\partial y}\right) - \frac{1}{\rho}\left(\frac{\partial h\tau_{xy}}{\partial x} - \frac{\partial h\tau_{yy}}{\partial y}\right) = 0 \qquad (A.3)$$

where:

h	= mean water depth	m
p, q	= volume transport in x- and y-direction	m^2/s
g	= acceleration due to gravity	ms^{-2}
z_b	= bottom level above reference level	m
τ_{sx}, τ_{sy}	= shear stress at the surface	N/m^2
τ_{bx}, τ_{by}	= bottom shear stress	N/m^2
ρ	= fluid density	kg/m^3
S_{xx} etc	= components of the wave action	N/m^2
τ_{xx} etc	= components of the effective stress	N/m^2

The general formulation for the effective stresses is given in [12]. The applied coefficients for bottomfriction, lateral mixing and wave action are specified for each condition in the text.

APPENDIX B ANALYSIS OF THE DRIVING MECHANISMS IN THE CURRENT FIELD

In order to obtain insight in the relation between the various driving mechanisms in the current field in a closed wave basin the current field will be subdivided into a first order and second order current field. The first order current field is related to oblique incident waves and an infinite long straight beach with parallel depth contours. The second order current field represents the additional current field due to the effects of a closed basin. If the coast is parallel to the x-axis then the following definitions can be used

$$u(x,y) = u_o(y) + u_1(x,y) \tag{B.1}$$

$$v(x,y) = v_1(x,y) \tag{B.2}$$

$$h(x,y) = h_o(y) + h_1(x,y) \tag{B.3}$$

$$z_b(x,y) = z_{bo}(y) \tag{B.4}$$

Remembering the definitions of p and q

$$p = uh \tag{B.5}$$

$$q = vh \tag{B.6}$$

then the following first and second order differential equations can be derived from (A.1) through (A.3).

first order equations

$$\frac{\partial h_o}{\partial t} + \frac{\partial}{\partial x}(u_o h_o) = 0 \tag{B.7}$$

$$\frac{\partial (u_o h_o)}{\partial t} + \frac{1}{\rho}\left(\frac{\partial S_{xx}}{\partial x} + \frac{\partial S_{xy}}{\partial y}\right) + C\,|u_{max}|\,u_o + - \frac{\partial}{\partial y}\left(h_o\,\varepsilon\,\frac{\partial u_o}{\partial y}\right) = 0 \tag{B.8}$$

$$\frac{1}{\rho}\left(\frac{\partial S_{xy}}{\partial x} + \frac{\partial S_{yy}}{\partial y}\right) + g\,h_o\left(\frac{\partial h_o}{\partial y} + \frac{\partial z_{bo}}{\partial y}\right) = 0 \tag{B.9}$$

second order equations

$$\frac{\partial h_1}{\partial t} + \frac{\partial}{\partial x}(u_o h_1 + h_o u_1) + \frac{\partial}{\partial y}(h_o v_1) = 0 \qquad \text{(B.10)}$$

$$\frac{\partial}{\partial t}(h_o u_1 + u_o h_1) + \frac{\partial}{\partial x}(2u_o h_o u_1 + u_o^2 h_1) + \frac{\partial}{\partial y}(u_o h_o v_1) +$$

$$+ g\, h_o \left(\frac{\partial}{\partial x} h_1 + \frac{\partial}{\partial x} z_{b1}\right) + C\,|u_{max}|\, u_1 +$$

$$- \frac{1}{\rho}\left\{\frac{\partial}{\partial x}\left(h_o\, \varepsilon \left(\frac{\partial u_1}{\partial x} - \frac{\partial v_1}{\partial y}\right)\right) + \frac{\partial}{\partial y}\left(h_o\, \varepsilon \left(\frac{\partial v_1}{\partial x} + \frac{\partial u_1}{\partial y}\right)\right) +\right.$$

$$\left. + \frac{\partial}{\partial y}\left(h_1\, \varepsilon \frac{\partial u_o}{\partial y}\right)\right\} = 0 \qquad \text{(B.11)}$$

$$\frac{\partial}{\partial t}(h_o v_1) + \frac{\partial}{\partial x}(u_o h_o v_1) + g\, h_1 \left(\frac{\partial h_o}{\partial y} + \frac{\partial z_{bo}}{\partial y}\right) +$$

$$+ g\, h_o \left(\frac{\partial h_1}{\partial y} + \frac{\partial z_{b1}}{\partial y}\right) + C\,|u_{max}|\, v_1 +$$

$$- \frac{1}{\rho}\left\{\frac{\partial}{\partial x} h_o\, \varepsilon \left(\frac{\partial v_1}{\partial x} + \frac{\partial u_1}{\partial y}\right) + \frac{\partial}{\partial y} h_o\, \varepsilon \left(\frac{\partial v_1}{\partial y} - \frac{\partial u_1}{\partial x}\right) +\right.$$

$$\left. + \frac{\partial}{\partial x}\left(h_1\, \varepsilon \frac{\partial u_o}{\partial y}\right) - \frac{\partial}{\partial y}\left(h_1\, \varepsilon \frac{\partial u_o}{\partial x}\right)\right\} = 0 \qquad \text{(B.12)}$$

APPENDIX C DERIVATION OF THE VORTICITY EQUATION IN STREAMWISE CO-ORDINATES

The equations of motion expressed in terms of u, v and h can be obtained from (A.2) and (A.3) by using the continuity equation and division by h. The resulting equations are

$$\frac{\partial h}{\partial t} + \frac{\partial (uh)}{\partial x} + \frac{\partial (vh)}{\partial y} = 0 \tag{C.1}$$

$$\frac{\partial u}{\partial t} + u\frac{\partial u}{\partial x} + v\frac{\partial u}{\partial y} + g\left(\frac{\partial h}{\partial x} + \frac{\partial z_b}{\partial x}\right) + \tau_{bx}/(\rho h) +$$

$$+ F_x/(\rho h) - \left\{\frac{\partial}{\partial x}(h\tau_{xx}) + \frac{\partial}{\partial y}(h\tau_{xy})\right\}/(\rho h) = 0 \tag{C.2}$$

$$\frac{\partial v}{\partial t} + u\frac{\partial v}{\partial x} + v\frac{\partial v}{\partial y} + g\left(\frac{\partial h}{\partial y} + \frac{\partial z_b}{\partial y}\right) + \tau_{by}/(\rho h) +$$

$$+ F_y/(\rho h) - \left\{\frac{\partial}{\partial x}(h\tau_{xy}) + \frac{\partial}{\partial y}(h\tau_{yy})\right\}/(\rho h) = 0 \tag{C.3}$$

where

$$F_x = \frac{\partial S_{xx}}{\partial x} + \frac{\partial S_{xy}}{\partial y} \tag{C.4}$$

$$F_y = \frac{\partial S_{yy}}{\partial y} + \frac{\partial S_{xy}}{\partial x} \tag{C.5}$$

The viscosity terms will be approximated for simplicity as follows

$$\frac{\partial}{\partial x}(h\tau_{xx}) + \frac{\partial}{\partial y}(h\tau_{xy}) \simeq h\left\{\frac{\partial \tau_{xx}}{\partial x} + \frac{\partial \tau_{xy}}{\partial y}\right\} \tag{C.6}$$

$$\frac{\partial}{\partial x}(h\tau_{xy}) + \frac{\partial}{\partial y}(h\tau_{yy}) \simeq h\left\{\frac{\partial \tau_{xy}}{\partial x} + \frac{\partial \tau_{yy}}{\partial y}\right\} \tag{C.7}$$

while ε will be assumed to be constant.
The vorticity will be defined as the anti-clockwise rotation of the diagonal of a fluid element

$$\omega = \frac{\partial v}{\partial x} - \frac{\partial u}{\partial y} \tag{C.8}$$

The vorticity equation in x and y terms can be obtained by taking the x-derivative of (C.3) and subtracting the y-derivative of (C.2). After

some rearrangement follows inside the breakerzone

$$\frac{\partial \omega}{\partial t} + \frac{\partial (u\omega)}{\partial x} + \frac{\partial (v\omega)}{\partial y}) + \frac{\partial}{\partial x} \{F_y/(\rho h)\} - \frac{\partial}{\partial y} \{F_x/(\rho h)\} +$$

$$+ \frac{\partial}{\partial x} \{\tau_{by}/(\rho h)\} - \frac{\partial}{\partial y} \{\tau_{bx}/(\rho h)\} - \frac{\varepsilon}{\rho} (\frac{\partial^2 \omega}{\partial x^2} + \frac{\partial^2 \omega}{\partial y^2}) = 0 \qquad (C.9)$$

It has been shown in paragraph 5.2 that outside the breakerzone the first order pressure terms balance the wave action term

$$\frac{1}{\rho} (\frac{\partial S_{xx}}{\partial x} + \frac{\partial S_{xy}}{\partial y}) + g\, h_o\, (\frac{\partial h_o}{\partial x} + \frac{\partial z_{bo}}{\partial x}) = 0 \qquad (C.10)$$

$$\frac{1}{\rho} (\frac{\partial S_{xy}}{\partial x} + \frac{\partial S_{yy}}{\partial y}) + g\, h_o\, (\frac{\partial h_o}{\partial y} + \frac{\partial z_{bo}}{\partial y}) = 0 \qquad (C.11)$$

This implies that outside the breakerzone the x-derivative of (C.11) and the y-derivative of (C.10) are zero. The x- and y-gradients of the second and higher order pressure terms cancel because of the asymmetry of these terms in the equations of motion. The vorticity equation outside the breakerzone becomes

$$\frac{\partial \omega}{\partial t} + \frac{\partial (u\omega)}{\partial x} + \frac{\partial (v\omega)}{\partial y} + \frac{\partial}{\partial x} \{\tau_{by}/(\rho h)\} - \frac{\partial}{\partial y} \{\tau_{bx}/(\rho h)\}$$

$$- \frac{\varepsilon}{\rho} (\frac{\partial^2 \omega}{\partial x^2} + \frac{\partial^2 \omega}{\partial y^2}) = 0 \qquad (C.12)$$

The convective terms can be rewritten as

$$\frac{\partial}{\partial x}(u\omega) + \frac{\partial}{\partial y}(v\omega) = \frac{1}{n} \{\frac{\partial}{\partial x}(uh\omega) + \frac{\partial}{\partial y}(vh\omega)\} +$$

$$- \frac{\omega}{h} \{u\frac{\partial h}{\partial x} + v\frac{\partial h}{\partial y}\} \qquad (C.13)$$

Define a stream function as follows

$$uh = \frac{\partial \psi}{\partial y} \qquad vh = - \frac{\partial \psi}{\partial x} \qquad (C.14)$$

then the first term on the right hand side of (C.13) can be rewritten as

$$\frac{1}{h}\{\frac{\partial}{\partial x}(uh\omega) + \frac{\partial}{\partial y}(vh\omega)\} = \frac{1}{h}\{\frac{\partial\psi}{\partial y}\frac{\partial\omega}{\partial x} - \frac{\partial\psi}{\partial x}\frac{\partial\omega}{\partial y}\} =$$

$$= -\frac{1}{h}\text{grad } \psi \text{ x grad } \omega = U\frac{\partial\omega}{\partial s} \qquad \text{(C.15)}$$

The second term of the right hand side of (C.13) follows similarly

$$u\frac{\partial h}{\partial x} + v\frac{\partial h}{\partial y} = \frac{1}{h}\{\frac{\partial\psi}{\partial y}\frac{\partial h}{\partial x} - \frac{\partial\psi}{\partial x}\frac{\partial h}{\partial y}\} =$$

$$-\frac{1}{h}\text{ grad } \psi \text{ x grad } h = U\frac{\partial h}{\partial s} \qquad \text{(C.16)}$$

The result of the convective terms in streamwise co-ordinates is according to (C.13), (C.15) and (C.16)

$$\frac{\partial}{\partial x}(u\omega) + \frac{\partial}{\partial y}(v\omega) = U\{\frac{\partial\omega}{\partial s} - \frac{\omega}{h}\frac{\partial h}{\partial s}\} = Uh\frac{\partial}{\partial s}(\frac{\omega}{h}) \qquad \text{(C.17)}$$

For the bottom friction a linear friction law will be assumed, while the wave motion will be approximated with the shallow water theory

$$\frac{1}{\rho}\tau_{bx} = \tfrac{1}{2}C\frac{H}{h}\sqrt{gh}\ u \qquad \text{(C.18)}$$

$$\frac{1}{\rho}\tau_{by} = \tfrac{1}{2}C\frac{H}{h}\sqrt{gh}\ v \qquad \text{(C.19)}$$

The bottom friction term in (C.9) becomes with (C.18) and (C.19)

$$\frac{\partial}{\partial x}\{\tau_{by}/(\rho h)\} - \frac{\partial}{\partial y}\{\tau_{bx}/(\rho h)\} = \tfrac{1}{2}C\ H\ g^{\frac{1}{2}}\{\frac{\partial}{\partial x}(v\ h^{-1\frac{1}{2}}) - \frac{\partial}{\partial y}(u\ h^{-1\frac{1}{2}})\} \qquad \text{(C.20)}$$

Using the same approach as before (C.20) can be written as

$$\frac{\partial}{\partial x}\{\tau_{by}/(\rho h)\} - \frac{\partial}{\partial y}\{\tau_{bx}/(\rho h)\} = \tfrac{1}{2}C\ (\frac{H}{h})(\frac{g}{h})^{\frac{1}{2}}\{\omega + \frac{3}{2}\frac{u}{h}\frac{\partial h}{\partial n}\} \qquad \text{(C.21)}$$

In the derivation use has been made of the following equality

$$v\frac{\partial h}{\partial x} - u\frac{\partial h}{\partial y} = -\frac{1}{h}\{\frac{\partial\psi}{\partial x}\frac{\partial h}{\partial x} + \frac{\partial\psi}{\partial y}\frac{\partial h}{\partial y}\} = -\frac{1}{h}(\text{grad } \psi.\ \text{grad } h) = -U\frac{\partial h}{\partial n} \qquad \text{(C.22)}$$

The resulting vorticity equation in streamwise co-ordinates using (C.9), (C.16) and (C.22) becomes

$$\frac{1}{(hU)}\frac{\partial\omega}{\partial t} + \frac{\partial}{\partial s}\left(\frac{\omega}{h}\right) + \left(\frac{\omega}{h}\right)\left\{\tfrac{1}{2}C\,\frac{H}{h}\,\frac{(gh)^{\frac{1}{2}}}{Uh}\right\} + \frac{3}{4}C\,\frac{H}{h}\,(gh)^{\frac{1}{2}}\,\frac{1}{h^3}\,\frac{\partial h}{\partial n} +$$

$$- \left(\frac{\varepsilon}{\rho hU}\right)\left(\frac{\partial^2\omega}{\partial x^2} + \frac{\partial^2\omega}{\partial y^2}\right) = 0 \qquad \text{(C.23)}$$

The viscosity term has not further been elaborated because in the application of (C.23) it will be assumed that ε is zero.

APPENDIX D VISCOUS CIRCULATION FLOW

The fluid motion in a steady circulation flow is governed by three elements

a viscosity
b bottom friction
c a constant velocity at the boundary.

This motion is comparable with the movement of the fluid in a rotating cylinder. This problem can easily be analysed in cylindrical co-ordinates.

radial velocity u_r

$$\frac{\partial u_r}{\partial t} + u_r \frac{\partial u_r}{\partial r} + \frac{u_\Theta}{r} \frac{\partial u_r}{\partial \Theta} - \frac{u_\Theta^2}{r} = - \frac{1}{\rho} \frac{\partial p}{\partial r} +$$

$$+ \nu \left(\nabla^2 u_r - \frac{u_r}{r^2} - \frac{2}{r^2} \frac{\partial u_\Theta}{\partial \Theta}\right) - c\, u_r \qquad (D.1)$$

tangential velocity u_Θ

$$\frac{\partial u_\Theta}{\partial t} + u_r \frac{\partial u_\Theta}{\partial r} + \frac{u_\Theta}{r} \frac{\partial u_\Theta}{\partial \Theta} + u_r \frac{u_\Theta}{r} = - \frac{1}{\rho r} \frac{\partial p}{\partial \Theta} +$$

$$+ \nu \left(\nabla^2 u_\Theta + \frac{2}{r^2} \frac{\partial u_r}{\partial \Theta} - \frac{u_\Theta}{r^2}\right) - c\, u_\Theta \qquad (D.2)$$

where

$$\nabla^2 v = \frac{1}{r} \frac{\partial}{\partial r} \left(r \frac{\partial v}{\partial r}\right) + \frac{1}{r^2} \frac{\partial^2 v}{\partial \Theta^2} \qquad (D.3)$$

For these equations of motion the following assumptions have been made:

- incompressible fluid
- no body force
- constant viscosity coefficient
- linear bottom friction law (c = constant).

For the two-dimensional stationary fluid motion in the rotating cylinder the following conditions will adhere

- no change of velocity with time ($\frac{\partial}{\partial t} = 0$)
- radial velocity is zero ($u_r = 0$)
- radial symmetric fluid motion ($\frac{\partial}{\partial \Theta} = 0$).

These conditions are applied to the equations (D.1) and (D.2) and lead to the following expressions

$$\frac{u_\Theta^2}{r} = \frac{1}{\rho} \frac{\partial p}{\partial r} \tag{D.4}$$

$$\nu \{\frac{1}{r} \frac{\partial}{\partial r}(r \frac{\partial u_\Theta}{\partial r}) - \frac{u_\Theta}{r^2}\} - c\, u_\Theta = 0 \tag{D.5}$$

The fluid motion follows from (D.5), while the slope of the mean water level can be obtained from (D.4).
The velocity u_θ is not a function of r only. Working out equation (D.5) yields after division by ν and multiplication by r .

$$r^2 \frac{d^2 u_\Theta}{dr^2} + r \frac{du_\Theta}{dr} - (1 + \frac{c}{\nu} r^2)\, u_\Theta = 0 \tag{D.6}$$

Introduce the following new variables

$$z = r(\frac{c}{\nu})^{\frac{1}{2}} \tag{D.7}$$

$$y\, u_o = u_\Theta \tag{D.8}$$

$$\text{where } u_\Theta = u_o \text{ if } r = R \tag{D.9}$$

From (D.6) follows

$$z^2 \frac{d^2 y}{dz^2} + z \frac{dy}{dz} - (z^2 + 1)\, y = 0 \tag{D.10}$$

This is a modified Bessel equation.